EUROPEAN ORGANIZATION FOR NUCLEAR RESEARCH

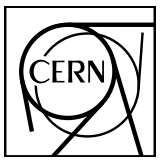

CERN-PH-EP-2013-205
02 November 2013

Measurement of charged jet suppression in Pb-Pb collisions at $\sqrt{s_{\rm NN}} = 2.76$ TeV

The ALICE Collaboration*

Abstract

The ALICE collaboration at the LHC reports a measurement of the transverse momentum spectra of jets in Pb–Pb collisions at $\sqrt{s_{\rm NN}} = 2.76$ TeV. Jets are reconstructed from charged particles using the anti-$k_{\rm T}$ jet algorithm with jet resolution parameters R of 0.2 and 0.3 in pseudo-rapidity $|\eta| < 0.5$. The transverse momentum $p_{\rm T}$ of charged particles is measured down to 0.15 GeV/c which gives access to the low $p_{\rm T}$ fragments of the jet. Jets found in heavy-ion collisions are corrected event-by-event for average background density and on an inclusive basis (via unfolding) for residual background fluctuations and detector effects. A strong suppression of jet production in central events with respect to peripheral events is observed. The suppression is found to be similar to the suppression of charged hadrons, which suggests that substantial energy is radiated at angles larger than the jet resolution parameter $R = 0.3$ considered in the analysis. The fragmentation bias introduced by selecting jets with a high $p_{\rm T}$ leading particle, which rejects jets with a soft fragmentation pattern, has a similar effect on the jet yield for central and peripheral events. The ratio of jet spectra with $R = 0.2$ and $R = 0.3$ is found to be similar in Pb–Pb and simulated PYTHIA pp events, indicating no strong broadening of the radial jet structure in the reconstructed jets with $R < 0.3$.

*See Appendix B for the list of collaboration members

1 Introduction

Discrete formulations of Quantum Chromodynamics (lattice QCD) predict a phase transition to a new state of matter, the Quark-Gluon Plasma (QGP), at an energy density above a critical value of about $1\,\mathrm{GeV/fm^3}$ and temperatures beyond $T_\mathrm{C} \approx 160$ MeV [1, 2]. In this state, the elementary constituents of hadronic matter, quarks and gluons, are deconfined and it is expected that chiral symmetry is restored. The conditions to create a QGP are expected to be reached for a short time (few fm/c) in the overlap region of heavy nuclei colliding at high energy.

One of the tools to study the properties of the QGP is provided by hard (large momentum transfer Q^2) scattering processes of the partonic constituents of the colliding nucleons. These hard scatterings occur early in the collision ($\ll 1\,\mathrm{fm}/c$) and the outgoing partons propagate through the expanding hot and dense medium and fragment into jets of hadrons. Jet fragmentation in heavy-ion collisions is expected to be modified (relative to the parton fragmentation in the vacuum) due to parton-medium interactions, e.g. radiative and collisional parton energy loss (jet quenching) [3,4]. The initial hard parton production cross sections are calculable using perturbative QCD (pQCD) and the non-perturbative vacuum fragmentation process can be well calibrated via jet measurements in elementary collisions.

Jet quenching has been observed at RHIC [5–10] and at the LHC [11–17] via the measurement of high-p_T inclusive hadron and jet production, di-hadron angular correlations and the energy imbalance of reconstructed dijets, which are observed to be strongly suppressed and modified, respectively, in central AA collisions compared to a pp (vacuum) reference. Single particle measurements provide limited information on the initial parton energy and its radiation. Jet reconstruction allows more direct access to the parton energies, which can be calculated using pQCD, by integrating over the hadronic degrees of freedom in a collinear and infrared safe way. Jets are reconstructed by grouping the detected particles within a given angular region, e.g. a cone with radius R. The interaction with the medium can result in a broadening of the jet profile with respect to vacuum fragmentation. In this case, for a given jet resolution parameter R and a fixed initial parton energy, the energy of the jet reconstructed in heavy-ion collisions will be smaller than in vacuum. In the case where the gluons are radiated inside the cone, the jet is expected to have a softer fragmentation and a modified density profile compared to jets in vacuum.

Jet measurements in heavy-ion collisions employ various approaches to correct for background energy not associated with jet production and to suppress the combinatorial, false jet yield induced by fluctuations of this background, e.g. via energy or momentum thresholds for particles that are used in the jet finding process. Each of these approaches represents a compromise between potential fragmentation biases in the jet reconstruction and a better separation of the jet signal from the background.

In this paper a measurement of the inclusive jet p_T spectrum in Pb–Pb collisions at $\sqrt{s_\mathrm{NN}} = 2.76$ TeV is reported in four centrality intervals in the most central 80% of the total hadronic cross-section. Jets are clustered from charged tracks measured with the central barrel detectors in ALICE down to momenta of $0.15\,\mathrm{GeV}/c$, which provides unique access to low p_T jet fragments at mid-rapidity at the LHC. Jets are measured with resolution parameters $R = 0.2$ and $R = 0.3$ in the pseudo-rapidity interval $-0.5 < \eta < 0.5$. The underlying event is subtracted event-by-event for each measured jet. The jet spectrum is corrected for background fluctuations and detector effects affecting the jet energy resolution and scale through an unfolding procedure.

The jet reconstruction strategy and the correction procedure for background from the underlying event is discussed in detail in Section 2 after which the results are presented in Section 3 and discussed in Section 4.

2 Data analysis and techniques

2.1 Data Sample and Event Selection

The data used for this analysis were recorded by the ALICE detector [18] in the fall of 2010 during the first Pb–Pb run at a collision energy of $\sqrt{s_{\rm NN}} = 2.76$ TeV. The analysis presented here uses minimum-bias events, which are selected online by requiring a signal in at least two out of the following three detectors: the forward VZERO counters (V0A and V0C) and the Silicon Pixel Detector (SPD) [19]. The VZERO counters are forward scintillator detectors covering a pseudo-rapidity range of $2.8 < \eta < 5.1$ (V0A) and $-3.7 < \eta < -1.7$ (V0C); the SPD is part of the Inner Tracking System (ITS) described below. The minimum-bias trigger is fully efficient in selecting hadronic events in Pb–Pb collisions. In addition, an offline selection is applied in which the online trigger is validated and remaining background events from beam-gas and electromagnetic interactions are rejected. To ensure a high tracking efficiency for all considered events, the primary vertex was required to be within 10 cm from the center of the detector along the beam axis and within 1 cm in the transverse plane.

The number of Pb–Pb events used in this analysis after event selection is 12.8 million in a centrality range between 0 and 80% most central of the total hadronic cross section, corresponding to a total integrated luminosity of 2 μb^{-1}. The event sample is divided in four centrality intervals (0–10%, 10–30%, 30–50%, and 50–80%) based on the sum of VZERO amplitudes. A Glauber model is used to calculate the number of participating nucleons $N_{\rm part}$ in the collisions, the number of binary collisions $N_{\rm coll}$, and the nuclear overlap function $T_{\rm AA}$ [19]. The resulting values and their uncertainties for the considered centrality intervals are given in Table 1.

Centrality	$\langle N_{\rm part} \rangle$	$\langle N_{\rm coll} \rangle$	$\langle T_{\rm AA} \rangle$
0–10%	356.0 ± 3.6	1500.5 ± 165.0	23.5 ± 0.8
10–30%	223.0 ± 3.5	738.8 ± 75.3	11.6 ± 0.4
30–50%	107.2 ± 2.8	245.6 ± 23.3	3.8 ± 0.2
50–80%	32.5 ± 1.2	45.9 ± 4.6	0.70 ± 0.04

Table 1: Average values of the number of participating nucleons $N_{\rm part}$, number of binary collisions $N_{\rm coll}$, and the nuclear overlap function $T_{\rm AA}$ for the centrality intervals used in the jet analysis. Experimental uncertainties on the parameters of the nuclear density profile used in the Glauber simulations and on the interpolated nucleon-nucleon cross section ($\sigma_{\rm inel}^{\rm NN} = 64 \pm 5$ mb) are included in the uncertainties. For details see [19].

2.2 Jet reconstruction

Jets were reconstructed using charged tracks detected in the Time Projection Chamber (TPC) [20] and the Inner Tracking System (ITS) [21] which cover the full azimuth and pseudo-rapidity $|\eta| < 0.9$. For each track traversing the TPC, up to 159 independent space points are measured at radial distances from 85 cm to 247 cm.

The ITS consists of six cylindrical silicon layers with high granularity for precision tracking, with the inner layer at 3.9 cm from the center of the detector and the outer layer at 43 cm. The measured space points in the ITS and the TPC are combined to reconstruct the tracks of charged particles. The transverse momentum is calculated from the measured track curvature in the magnetic field of $B = 0.5$ T.

The main track selection criteria are a minimum number of points in the TPC, a χ^2 cut on the fit, and a cut on the difference between the parameters of the track fit using all the space points in ITS and TPC, and using only the TPC space points with the primary vertex position as an additional constraint. Tracks for which the total change in the track parameters is more than 6σ ($\chi^2 > 36$) are rejected from the sample. For a large fraction (79%) of the tracks used in the analysis, at least one point was found in one of the two inner pixel tracking layers (SPD) of the ITS. To improve the azimuthal uniformity of the selected

tracks, tracks without SPD points were also used in the analysis. For those tracks the momentum was determined from a track fit constrained to the primary vertex, to guarantee good momentum resolution.

The p_{T} resolution for tracks is estimated from the track residuals of the momentum fit and does not vary significantly with centrality. All track types have a relative transverse momentum resolution of $\sigma(p_{\mathrm{T}})/p_{\mathrm{T}} \simeq 1\%$ at 1 GeV/c. The resolution at $p_{\mathrm{T}} = 50$ GeV/c is $\sigma(p_{\mathrm{T}})/p_{\mathrm{T}} \simeq 10\%$ for tracks that have at least three out of six reconstructed space points in the ITS. For the remaining tracks (6% of the track sample) the resolution is $\sigma(p_{\mathrm{T}})/p_{\mathrm{T}} \simeq 20\%$ at 50 GeV/c.

The track finding efficiency at $p_{\mathrm{T}} = 0.15$ GeV/c is 60% increasing to $\sim 90\%$ for $p_{\mathrm{T}} \simeq 1.5$ GeV/c and then decreases to $\sim 86\%$ for $p_{\mathrm{T}} \geq 2.5$ GeV/c. In peripheral events the track finding efficiency is $\sim 2\%$ larger than in central collisions due to the lower track multiplicity.

Jets are reconstructed with the anti-k_{T} algorithm using the FastJet package [22, 23] with resolution parameters $R = 0.2$ and $R = 0.3$. Charged tracks with $|\eta| < 0.9$ and $p_{\mathrm{T}} > 0.15$ GeV/c are used as input for the jet algorithm. The transverse momentum of the jets, $p_{\mathrm{T,ch\,jet}}^{\mathrm{raw}}$, is calculated with the boost-invariant p_{T} recombination scheme. The area, A, for each jet is determined using the active area method as implemented in FastJet [24]. So-called 'ghost particles' with very small momentum ($\sim 10^{-100}$ GeV/c) are added to the event and the number of ghost particles in a jet measures the area. Ghost particles are uniformly generated over the tracking acceptance ($0 < \varphi < 2\pi$ and $|\eta| < 0.9$), with 200 ghost particles per unit area. Jets used in the analysis are required to have an area larger than 0.07 for $R = 0.2$ jets and 0.2 for $R = 0.3$ jets. This selection mostly removes low momentum jets with $p_{\mathrm{T,ch\,jet}}^{\mathrm{raw}} < 20$ GeV/c. Jets are selected to have $|\eta| < 0.5$, so that they are fully contained in the tracking acceptance. In addition, jets containing a track with $p_{\mathrm{T}} > 100$ GeV/c, for which the momentum resolution is worse than 20%, are tagged and rejected after performing the jet clustering. This selection has negligible effect in the reported range of jet momenta.

2.3 Background subtraction

In Pb–Pb events, the large background consisting of particles from soft scattering processes as well as fragments from other jets, is subtracted using the procedure proposed in [25, 26]. The background is measured on an event-by-event basis by clustering all particles using the k_{T}-algorithm and determining the median of the transverse momentum density $\rho_{\mathrm{ch}}^{i} = p_{\mathrm{T,ch\,jet}}^{i}/A^{i}$ of all clusters i in the event, excluding the two leading clusters to limit the impact of the hard jet signal on the background estimate. The signal anti-k_{T} jets are then corrected for the average background contribution using the median ρ_{ch}:

$$p_{\mathrm{T,ch\,jet}} = p_{\mathrm{T,ch\,jet}}^{\mathrm{raw}} - \rho_{\mathrm{ch}}\, A, \tag{1}$$

with $p_{\mathrm{T,ch\,jet}}$ the background subtracted jet p_{T}, $p_{\mathrm{T,ch\,jet}}^{\mathrm{raw}}$ the uncorrected measured jet p_{T} and A the area of the anti-k_{T} signal jet. The inclusive jet distribution is then corrected via unfolding to account for background fluctuations and detector effects.

As demonstrated in [27] the measured background density ρ_{ch} is directly related to the multiplicity and average transverse momentum of the reconstructed charged particles. Since it is based on the same collection of input particles used for the signal jets, the quantity ρ_{ch} used in the analysis intrinsically includes all detector effects, such as tracking efficiency and momentum resolution. To enable comparisons with other experiments and generator studies, the corrected background momentum density is obtained using the Hit-Backspace-Once-More (HBOM) method proposed in [28], i.e. by repeatedly applying the parameterized detector response to the measured heavy-ion events and extrapolating the measured ρ to an ideal detector. The advantage of the method lies in the data-driven approach where only the detector response is taken from simulation. This is of particular importance when studying observables that are sensitive to the a-priori unknown structure of the heavy-ion event and the correlation between different regions in the event. This procedure yields a corrected transverse momentum density of $\rho_{\mathrm{ch}}^{p_{\mathrm{T}}>0.15} = 155.8 \pm 3.7$

GeV/c for the 10% most central events, with a spread $\sigma(\rho_{\rm ch}^{p_{\rm T}>0.15}) = 20.5 \pm 0.4$ GeV/c with no significant dependence on the distance parameter R employed in the ρ calculation.

2.4 Background fluctuations

All particles created in a collision are clustered into jets, but not all of them originate from hard processes. The distinction between jets originating from a hard parton and soft clusters containing mostly background particles (*combinatorial jets*) is to some extent arbitrary and requires a pragmatic definition. At very high $p_{\rm T}$, it is clear that all jets originate from parton fragmentation processes, while at low and intermediate $p_{\rm T}$, clusters can be formed by including fragments from multiple, independent parton scatterings or even from the soft hadronization.

Jet clusters which originate from a hard scattering will contain a large amount of uncorrelated, mostly soft, background particles. The background subtraction procedure described in Section 2.3, removes the background energy *on average*, but the background has large region-to-region fluctuations in the event, both due to statistical fluctuations of the particle number and momentum, and collective phenomena like elliptic flow.

Combinatorial jets and background fluctuations are intimately related: low energy jets, for example with a momentum below 5 GeV/c, are also subject to background fluctuations and appear at relatively high $p_{\rm T}$ (well above 20 GeV/c). Such jets are mostly background energy, and thus background fluctuations give rise to combinatorial jets.

For the results reported in the next sections an unfolding procedure is used to correct for background fluctuations. In this procedure, the combinatorial jets will emerge at low $p_{\rm T}$, while the spectrum is only reported above a certain $p_{\rm T}$ cut-off, thus effectively removing the combinatorial jets from the result.

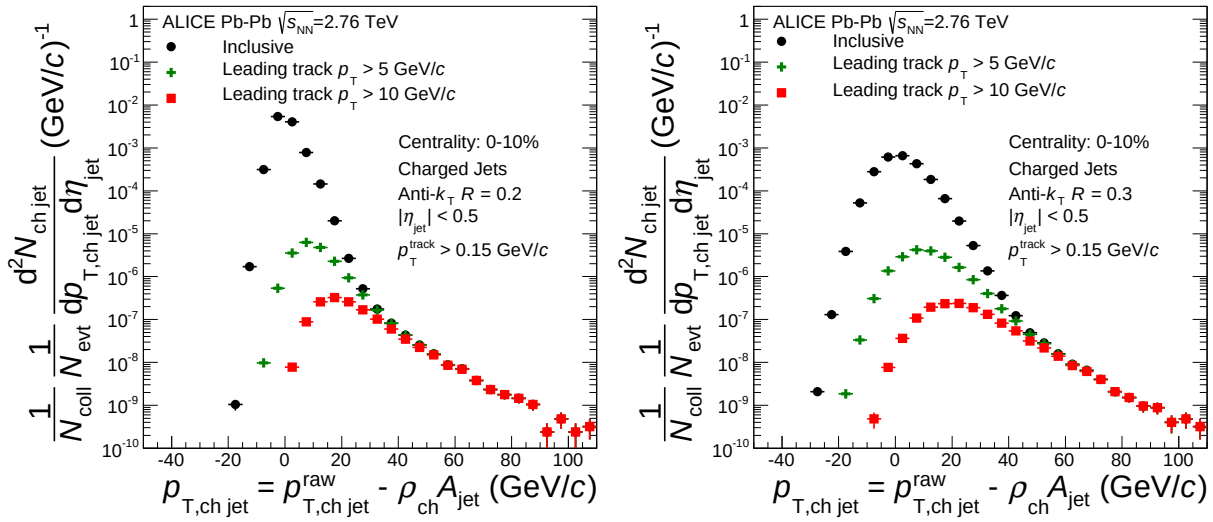

Fig. 1: Uncorrected jet spectra after background subtraction, with radius parameters $R = 0.2$ (left) and $R = 0.3$ (right) in central Pb–Pb events, without leading particle selection (*unbiased*, black circles) and with at least one particle with $p_{\rm T} > 5$ (green crosses) or 10 GeV/c (red squares).

To illustrate the impact of combinatorial jets, Fig. 1 shows uncorrected jet spectra after event-by-event subtraction of the background following Eq. 1. The black solid circles show the result without further selection of the jets, which shows a broad peak around $p_{\rm T,ch\,jet} = 0$ GeV/c. A large fraction of the combinatorial jets can be removed by selecting jets with a leading charged particle above a certain threshold [29]. The crosses and squares in Fig. 1 show the jet spectra with a leading charged particle above 5 and 10 GeV/c. It can be seen clearly that selecting jets by a leading high $p_{\rm T}$ particle reduces the back-

ground contribution for $p_{\mathrm{T,ch\,jet}} < 40$ GeV/c. However, this selection does not only reject combinatorial jets, but also introduces a bias towards harder fragmentation.

In the following, unbiased and leading track biased jet spectra are reported. The systematic uncertainty arising from the combinatorial jet correction by unfolding is smaller for the biased spectra (for details, see Section 2.7).

Fluctuations of the background are quantified by placing cones with $R = 0.2$ and $R = 0.3$ at random locations within the acceptance of the measured Pb–Pb events ($0 < \varphi < 2\pi$ and $|\eta_{RC}| < 0.5$). The transverse momentum of charged particles in the Randomly positioned Cone (RC) is summed and the difference $\delta p_{\mathrm{T}}^{\mathrm{ch}} = \sum_i^{\mathrm{RC}} p_{\mathrm{T,i}} - \rho_{\mathrm{ch}} A$ is calculated, which represents the statistical (region-to-region) fluctuations of the background. An alternative method to quantify the background fluctuations is also used in which high p_{T} probes are embedded into the Pb–Pb events [27]. The events with embedded probes are clustered with the anti-k_{T} jet finder and the transverse momentum $p_{\mathrm{T,ch\,jet}}$ containing the embedded probe in the heavy-ion environment is compared to the embedded transverse momentum $p_{\mathrm{T}}^{\mathrm{probe}}$ by calculating the difference $\delta p_{\mathrm{T}}^{\mathrm{ch}} = p_{\mathrm{T,ch\,jet}}^{\mathrm{raw}} - \rho_{\mathrm{ch}} A - p_{\mathrm{T}}^{\mathrm{probe}}$.

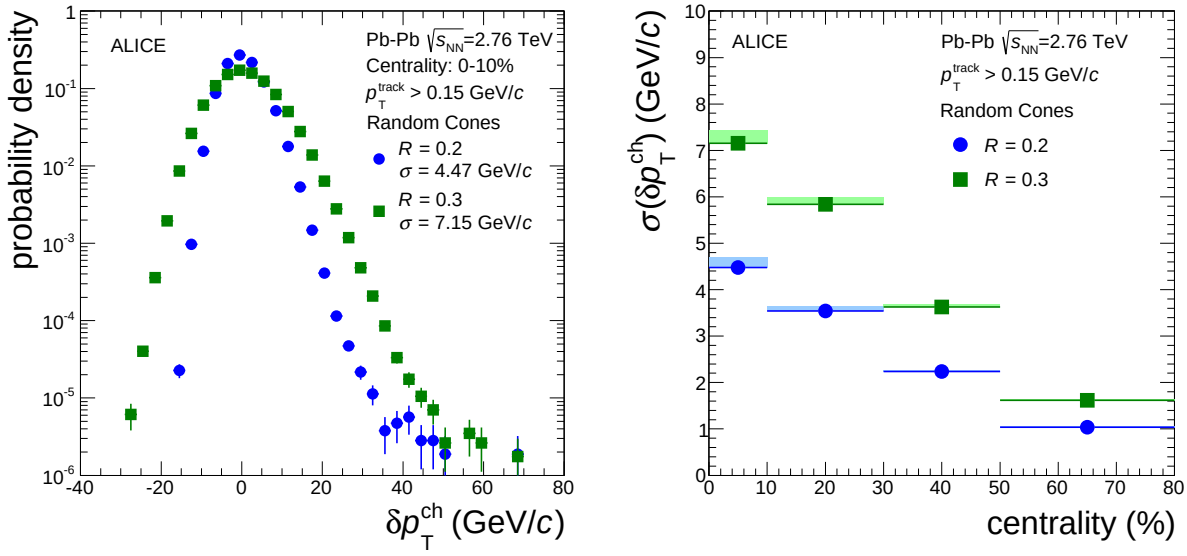

Fig. 2: Left: $\delta p_{\mathrm{T}}^{\mathrm{ch}}$ distribution for jets with resolution parameter $R = 0.2$ and $R = 0.3$ measured with random cones in central collisions. Right: Width of the background fluctuation $\delta p_{\mathrm{T}}^{\mathrm{ch}}$ distribution as a function of centrality for cone radii $R = 0.2$ and $R = 0.3$. The shaded uncertainty bands indicate the difference between the width of the $\delta p_{\mathrm{T}}^{\mathrm{ch}}$ distribution from random cones and high p_{T} probe embedding.

The left panel of Fig. 2 shows the $\delta p_{\mathrm{T}}^{\mathrm{ch}}$ distribution from the 10% most central events for the two jet resolution parameters used in this analysis. The standard deviation of the background fluctuations, $\sigma(\delta p_{\mathrm{T}}^{\mathrm{ch}})$, is 4.47 GeV/$c$ for $R = 0.2$ jets and 7.15 GeV/c for $R = 0.3$ jets (the statistical uncertainties are less than 4 MeV/c due to the large sample of random cones). The right panel of Fig. 2 shows the evolution of $\sigma(\delta p_{\mathrm{T}}^{\mathrm{ch}})$ with centrality for the two jet resolution parameters extracted with the random cones technique. The upper edge of the shaded boxes indicates the $\sigma(\delta p_{\mathrm{T}}^{\mathrm{ch}})$ obtained with track embedding, where single tracks with $20 < p_{\mathrm{T}}^{\mathrm{track}} < 110$ GeV/c were embedded in the heavy-ion events. The small increase in the standard deviation for more central events is due to the finite jet area resolution in the embedding [27].

Due to the asymmetry of the $\delta p_{\mathrm{T}}^{\mathrm{ch}}$ distribution, fluctuations that increase the jet energy are more probable than fluctuations to lower jet energy. More importantly, the steeply falling p_{T}-spectrum favours low-p_{T} jets with upward fluctuations over downward fluctuations of high-p_{T} jets at a given p_{T}.

Fluctuations of the background depend strongly on the multiplicity, jet area (or radius), and minimum

$p_{\rm T}$ of the measured particles [27]. The analysis presented here is limited to $R = 0.2$ and $R = 0.3$ to avoid instabilities in the correction which are present for larger radii, see also Section 2.6.

The measured (uncorrected) $\delta p_{\rm T}^{\rm ch}$ distributions are used directly to correct the jet spectrum for background fluctuations. In addition, the magnitude of background fluctuations also provides a potentially important characteristic of the properties of the heavy-ion event and the region-to-region variation of the transverse momentum density. For this purpose, the measured values were corrected using the same iterative procedure as for the background density ρ, *i.e.* applying the parameterized detector effects multiple times and extrapolating the fluctuations to an ideal detector [28]. Since the correction is based on the properties of the measured heavy-ion event, it takes into account all correlations in the event. The corrected width of the $\delta p_{\rm T}^{\rm ch}$ distribution is given in Table 2 for central collisions and various cone radii. The FastJet package provides a measure of fluctuations, $\sigma_{\rm FJ}$, which is defined from the distribution of individual jet momentum densities $p^i_{\rm T,ch\,jet}/A^i$ such that 15.9% of all clusters within an event satisfy $p^i_{\rm T,ch\,jet}/A^i < \rho - \sigma_{\rm FJ}\sqrt{A}$ [30]. This measure corrects to first order the area dependence of fluctuations ($\sigma \propto \sqrt{A}$), but is not sensitive to the tail of the distribution. The $\sigma_{\rm FJ}$ obtained with different radius parameters for the $k_{\rm T}$ jet finder and extrapolated to an ideal detector for charged particles above $p_{\rm T} > 0.15$ GeV/c is also reported in Table 2. It is multiplied by $\sqrt{\pi R^2}$ to re-introduce part of the area dependence, present in $\sigma(\delta p_{\rm T}^{\rm ch})$. The FastJet fluctuation measures are reported to enable the comparison of fluctuations in heavy ion reactions by standard jet reconstruction tools in models and data.

	$\sigma(\delta p_{\rm T}^{\rm ch})$		$\sigma_{\rm FJ}\cdot\sqrt{\pi R^2}$
	for $p_{\rm T}^{\rm track} > 0.15$ GeV/c in 10% most central events		
	Measured	Corrected	Corrected
$R = 0.2$	4.47 ± 0.00 GeV/c	5.10 ± 0.05 GeV/c	4.04 ± 0.05 GeV/c
$R = 0.3$	7.15 ± 0.00 GeV/c	8.21 ± 0.09 GeV/c	6.35 ± 0.09 GeV/c
$R = 0.4$	10.17 ± 0.01 GeV/c	11.85 ± 0.14 GeV/c	8.59 ± 0.12 GeV/c

Table 2: Measured and corrected width of the $\delta p_{\rm T}^{\rm ch}$ distribution for different cone radii. In addition, the corrected fluctuation measure from FastJet is provided, multiplied by $\sqrt{\pi R^2}$ to take into account the expected area dependence of the fluctuations. The values for $R = 0.4$ are given for comparison with [27].

2.5 Detector effects

The jet response in the ALICE detector is evaluated using simulations with the PYTHIA6 [31] event generator and GEANT3 [32] for detector response, using the same reconstruction software settings that are used for the reconstruction of Pb–Pb events. The effect of the high track density in Pb–Pb events on the tracking efficiency was studied using HIJING [33] events with the GEANT3 detector simulation. It is found that the tracking efficiency is a few per cent lower in central Pb–Pb collisions than in peripheral collisions and pp collisions. This additional centrality-dependent inefficiency was introduced to the PYTHIA events by a random rejection of tracks.

The jet response is determined on a jet-by-jet basis by comparing jets before (particle level jets) and after detector simulation (detector level jets), that are geometrically matched. In this analysis the detector to particle level correction is based on the Perugia-0 tune [34] of PYTHIA6. It was verified that the simulated detector response for jets is largely independent of the generator tune. No correction for hadronization effects was applied since the relation between parton level jet and particle level jet in heavy-ion collisions is not well-defined.

The detector effects that influence the jet energy scale and resolution are the charged particle tracking efficiency and the transverse momentum resolution, with the tracking efficiency being the dominant

contributor. The finite p_{T} resolution of reconstructed charged tracks has a small effect on the jet energy resolution since the majority of the constituents of a jet are of moderate p_{T} where the tracking momentum resolution is good. In addition, since the transverse momentum of the jet is the sum of the transverse momentum of independently measured tracks, the relative momentum resolution is in general better than that of individual tracks.

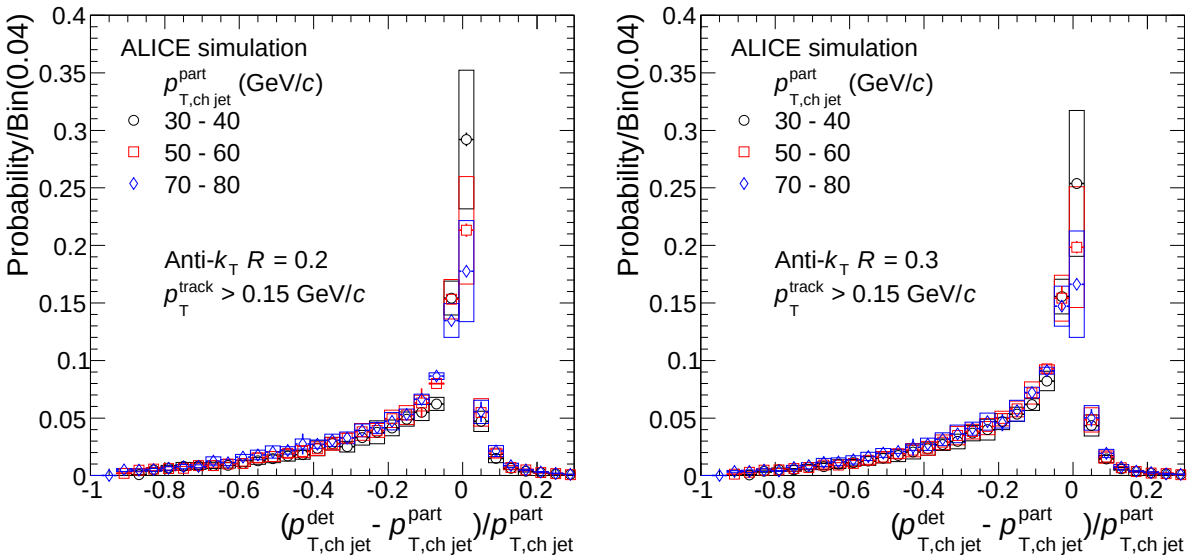

Fig. 3: Distribution of relative transverse momentum difference between detector and particle level anti-k_{T} jets with $R = 0.2$ and $R = 0.3$ and several ranges of jet transverse momentum at particle level. Distribution correspond to the 10% most central events. Events were generated using PYTHIA with the standard ALICE detector response simulation using GEANT3 and the data reconstruction algorithms and settings used for Pb–Pb events. The dominant systematic uncertainty is the uncertainty on tracking efficiency.

Figure 3 shows the probability distribution of the relative transverse momentum difference between the detector and particle level jets with resolution parameters $R = 0.2$ and $R = 0.3$ in three different intervals of the transverse momentum of the particle level jet $p^{\mathrm{part}}_{\mathrm{T,ch\,jet}}$. The most probable detector level $p^{\mathrm{det}}_{\mathrm{T,ch\,jet}}$ is very close to the particle level jet $p^{\mathrm{part}}_{\mathrm{T,ch\,jet}}$ in all cases. The average momentum of the detector level jet is lower than the particle level momentum, because of the average inefficiency of 10-20% in the charged particle reconstruction. Momentum resolution effects and under-subtraction of the background (back reaction) can cause a detector level jet to have a higher momentum. The momentum difference distribution is highly asymmetric and cannot be described by a Gaussian distribution.

To characterize the detector response, the mean of the relative difference between $p^{\mathrm{det}}_{\mathrm{T,ch\,jet}}$ and $p^{\mathrm{part}}_{\mathrm{T,ch\,jet}}$ as a function of the jet momentum at particle level is shown in Fig. 4. For unbiased jets the reconstructed jet momentum is on average 14–19% lower than the generated momentum, in the range $p^{\mathrm{part}}_{\mathrm{T,ch\,jet}} = 20 - 100$ GeV/c, with a weak p_{T}-dependence. The mean of the jet response is also shown for leading track biased jets with $p^{\mathrm{leading\ track}}_{\mathrm{T}} > 5$ and 10 GeV/c. Those jets whose leading track is not reconstructed in the detector are rejected from the sample. This results in an improved jet energy resolution at low jet p_{T} while the jet finding efficiency is decreased, as shown in Fig. 5.

To give more details on the detector response to jets, the most probable value of the relative difference between $p^{\mathrm{part}}_{\mathrm{T,ch\,jet}}$ and $p^{\mathrm{det}}_{\mathrm{T,ch\,jet}}$ is shown as a function of $p^{\mathrm{part}}_{\mathrm{T,ch\,jet}}$ in the right panel of Fig. 4. The most probable value is determined as the mean of a Gaussian function fitted to the peak region, $-0.03 < (p^{\mathrm{det}}_{\mathrm{T,ch\,jet}} - p^{\mathrm{part}}_{\mathrm{T,ch\,jet}})/p^{\mathrm{part}}_{\mathrm{T,ch\,jet}} < 0.03$. The most probable value of the detector level p_{T} is within 0.5% of $p^{\mathrm{part}}_{\mathrm{T,ch\,jet}}$over the entire p_{T} range.

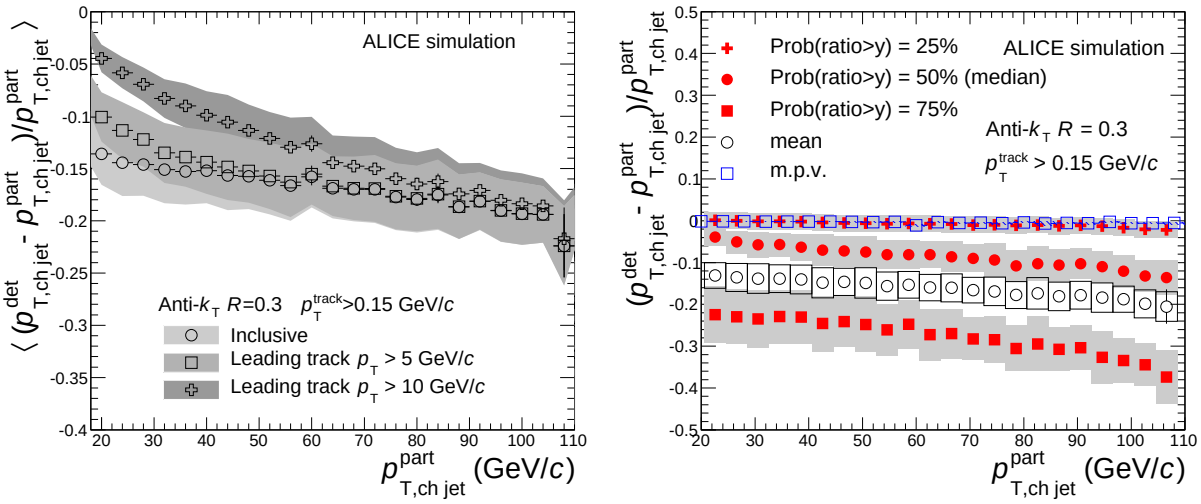

Fig. 4: Jet detector response for jet finding resolution parameter $R = 0.3$ for the 10% most central events. Data points extracted from event and full detector simulation. Systematic uncertainty originates from the uncertainty on the tracking efficiency. Left: mean of the jet response for charged jets with $R = 0.3$. See text for details. Right: Mean, most probably value and quartiles of the jet response as a function of jet momentum.

The right panel in Fig. 4 also shows the boundaries at 25%, 50% or 75% of the response distribution for jets with $R = 0.3$, integrating from the right $p_{\rm T,ch\,jet}^{\rm det} \to \infty$. Approximately 25% of the detector level jets has a larger reconstructed jet momentum than generated. The 50% percentile (median) correction is 5% at $p_{\rm T,ch\,jet}^{\rm part} = 20$ GeV/c and increases to 14% at $p_{\rm T,ch\,jet}^{\rm part} = 100$ GeV/c. For 75% of the jet population the correction for detector effects is smaller than 22% at low $p_{\rm T,jet} \approx 20\,$GeV/$c$ and 30% at high $p_{\rm T,jet} \approx 100\,$GeV/$c$.

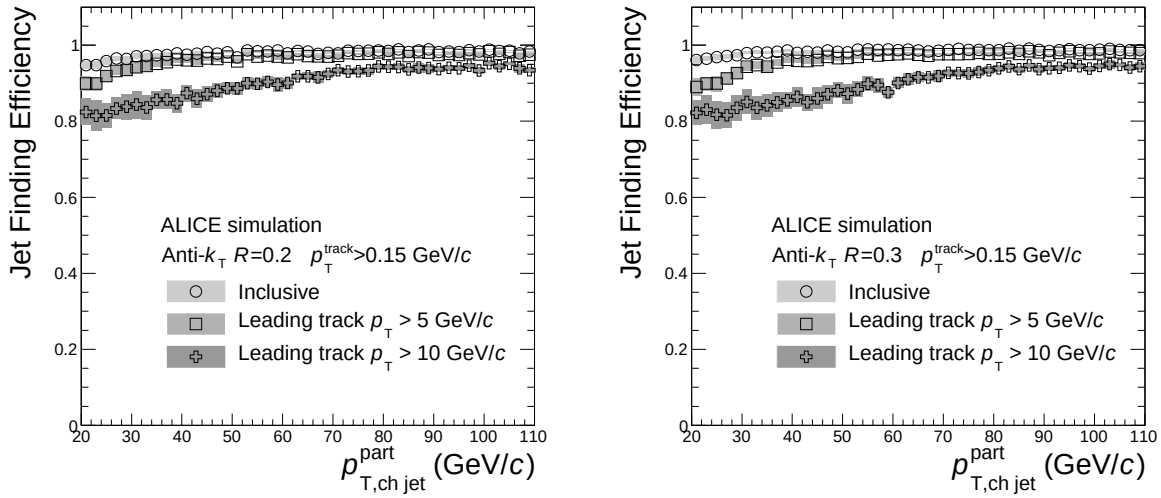

Fig. 5: Jet-finding efficiency for inclusive unbiased and leading track biased jets extracted from event and detector simulation for the 10% most central events. Left panel: $R = 0.2$. Right panel: $R = 0.3$.

The jet-finding efficiency is obtained by taking the ratio between the spectra of the particle level jets which have a detector level partner, and all particle level jets. In case of jets biased by a high $p_{\rm T}$ constituent, the numerator consists of jets fulfilling the high $p_{\rm T}$ track requirement on detector level and the denominator are all particle level jets with a high $p_{\rm T}$ generated particle. Figure 5 shows the jet-finding efficiency for the unbiased sample, which is unity at high $p_{\rm T}$ and reduces to 95% at $p_{\rm T,ch\,jet}^{\rm part} = 20$ GeV/c

due to migration of the jet axis outside the η acceptance. The jet-finding efficiency for jets with radii of $R = 0.2$ and $R = 0.3$ differs by a few percent at low p_{T} and is the same at high p_{T}. In general the jet-finding efficiency is ∼1% higher in pp compared to Pb–Pb without a p_{T} dependence for $p_{\mathrm{T,ch\,jet}}^{\mathrm{part}} > 20$ GeV/c. For leading track biased jets, the jet-finding efficiency is reduced and reaches 90% at $p_{\mathrm{T,ch\,jet}}^{\mathrm{part}} \approx 25$ GeV/c for $p_{\mathrm{T}}^{\mathrm{leading\,track}} > 5$ GeV/c and at $p_{\mathrm{T,ch\,jet}}^{\mathrm{part}} \approx 60$ GeV/c for $p_{\mathrm{T}}^{\mathrm{leading\,track}} > 10$ GeV/c, which is consistent with the charged particle tracking efficiency.

2.6 Unfolding

Both background fluctuations and detector effects lead to smearing of the measured jet momentum in heavy ion collisions. These effects can be corrected for using deconvolution, or *unfolding* procedures [35–37]. The background fluctuations and detector effects partially compensate: an upward energy shift is more likely due to background fluctuations while detector effects mainly induce a shift to lower p_{T}.

The relation between the measured spectrum $\mathbf{M}_m$ and the 'true' jet spectrum $\mathbf{T}_t$ is

$$\mathbf{M}_m = \mathbf{R}_{m,t}^{\mathrm{tot}} \cdot \mathbf{T}_t = \mathbf{R}_{m,d}^{\mathrm{bkg}} \cdot \mathbf{R}_{d,t}^{\mathrm{det}} \cdot \mathbf{T}_t, \tag{2}$$

where $\mathbf{R}_{d,t}^{\mathrm{det}}$ is the response matrix for detector effects (including efficiencies), $\mathbf{R}_{m,d}^{\mathrm{bkg}}$ is the response matrix for background fluctuations, and $\mathbf{R}_{m,t}^{\mathrm{tot}} = \mathbf{R}_{m,d}^{\mathrm{bkg}} \cdot \mathbf{R}_{d,t}^{\mathrm{det}}$ is the total response matrix for the combined effects of background fluctuations and detector effects. The subscripts m, d, t are indices indicating the bin number.

The response for background fluctuations is extracted with the data-driven method described in Section 2.4 and the response for detector effects is obtained from detector simulations as described in Section 2.5. The response matrices are combined into an overall response matrix $\mathbf{R}_{m,t}^{\mathrm{tot}}$. It was verified that correcting for detector effects and background fluctuations in two separate unfolding steps yields the same unfolded jet spectrum.

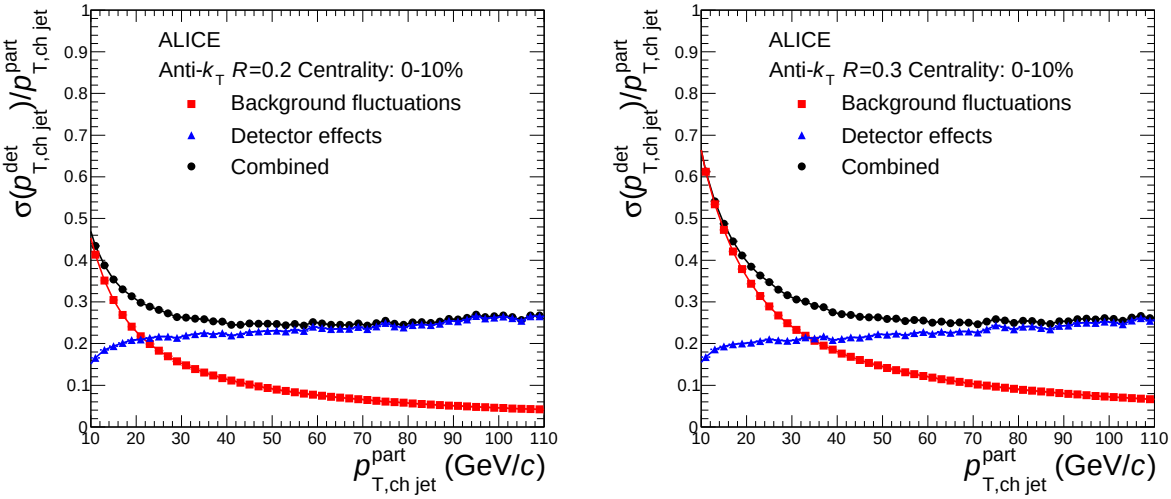

Fig. 6: Combined jet response for charged jets for the two resolution parameters considered, including background fluctuations and detector effects for 0-10% central Pb–Pb events. Left panel: $R = 0.2$. Right panel: $R = 0.3$.

Figure 6 shows the width of the combined response $\sigma(p_{\mathrm{T,ch\,jet}}^{\mathrm{det}})/p_{\mathrm{T,ch\,jet}}^{\mathrm{part}}$ as a function of $p_{\mathrm{T,ch\,jet}}^{\mathrm{part}}$. It can be observed that the dominant correction at low momenta originates from the background fluctuations while at high p_{T} the detector effects dominate.

Inverting Eq. 2 to obtain the true spectrum from the measured spectrum requires some care: calculating the inverse of the response matrix leads to solutions for the true jet spectrum that has large unphysical

bin-to-bin-fluctuations. To suppress these fluctuations, unfolding algorithms implement regularisation procedures, which impose a smoothness criterion on the final result. There is some freedom in the choice of regularisation procedure, which leads to an additional systematic uncertainty on the unfolded spectrum for the final result.

Three unfolding algorithms with different regularisation procedures were tested: the χ^2 method with a log-log-regularisation (see Appendix A), the (generalized) Singular Value Decomposition (SVD) method as implemented in RooUnfold, and the Bayesian method [36, 38–41]. It was found in a closure test with a thermal background model that the Bayesian method does not converge properly for this case, while the other two methods give similar results. The covariance matrix $\mathrm{cov}(x,y)$ for the unfolded result is calculated by propagating the measurement errors in the unfolding and/or using Monte Carlo variations of the input spectra [41]. The quality of the unfolded result is evaluated by inspecting the Pearson coefficients $\rho(x,y) = \frac{\mathrm{cov}(x,y)}{\sigma_x \sigma_y}$. A large (anti-)correlation between neighboring bins indicates that the regularisation is too strong or too weak. The statistical uncertainties on the unfolded data points are the square root of the diagonal elements of the covariance matrix of the unfolded spectrum.

2.6.1 Unfolding strategy – $p_{\rm T}$ ranges

There are two relevant kinematic ranges in the unfolding strategy applied in this analysis: the $p_{\rm T}$-range of the measured spectrum and the $p_{\rm T}$-range of the unfolded spectrum, which may be different. A minimum $p_{\rm T}$ cut-off on the measured jet spectrum is introduced to suppress jet candidates, which are dominated by background fluctuations, including combinatorial jets, while the unfolded spectrum starts at the lowest possible $p_{\rm T}$, $p_{\rm T}^{\rm unfolded} > 0$ GeV/c.

The minimum $p_{\rm T}$ cut-off ($p_{\rm T}^{\rm min,meas}$) on the measured spectrum removes a large fraction of combinatorial jets, which makes the unfolding procedure more stable. Feed-in from true jets with $p_{\rm T} < p_{\rm T}^{\rm min,meas}$ into the region used for unfolding is accounted for by extending the unfolded spectrum to $p_{\rm T,ch\,jet} = 0$ GeV/c. The feed-in from low $p_{\rm T}$ true jets is a significant effect since the spectrum falls steeply with $p_{\rm T,ch\,jet}$. Combinatorial jets still present in the measurement after applying the kinematical selections are transferred in the unfolding procedure to the region below $p_{\rm T}^{\rm min,meas}$. Feed-in from jets with $p_{\rm T,ch\,jet}$ larger than the maximum measured $p_{\rm T,ch\,jet}$ is also included by extending the reach of the unfolded spectrum to $p_{\rm T,ch\,jet} = 250$ GeV/c. The optimal value of the minimum $p_{\rm T}$ cut-off has been studied using the jet background model described in [29] and within simpler set-up in which a jet spectrum is folded with the measured background fluctuations. Stable unfolding is obtained with a minimum $p_{\rm T}$ cut-off of at least five times the width of the $\delta p_{\rm T}^{\rm ch}$-distribution $\sigma(\delta p_{\rm T}^{\rm ch})$. For the most central collisions and $R = 0.3$, this means that the spectrum is reported for $p_{\rm T,ch\,jet} > 40$ GeV/c. In addition, the maximum $p_{\rm T}$ cut-off is driven by the available statistics. The present data set allows for a measurement of $p_{\rm T,ch\,jet} < 110$ GeV/c in central events and $p_{\rm T,ch\,jet} < 90$ GeV/c in peripheral events. In case of leading track biased jets, the unfolding is more stable since the correction for combinatorial jets is reduced.

2.7 Systematic uncertainties

The systematic uncertainties on the results were evaluated by varying a number of key assumptions in the correction procedure and by using different unfolding methods. The different tests and the resulting systematic uncertainties are discussed in the following subsections, and summerized in Table 3.

2.7.1 Unfolding and regularisation uncertainties

The uncertainties from the regularisation and the unfolding procedure were evaluated by changing the regularisation strength β in the χ^2-method and by comparing the results from the χ^2 method and the generalised SVD method. Both variations give an uncertainty on the applied regularisation. Therefore, the uncertainties were taken to be the maximum deviation from both studies. The SVD method also

makes use of a prior, which was varied. This has a negligible effect on the result.

Regularisation strength β The regularisation strength β (see Eq. A.2) is varied from a value where fluctuating solutions dominate to the point where the unfolding becomes over-constrained. The main effect of varying β is that the unfolded jet spectrum changes shape. With increasing regularisation, the unfolded spectrum becomes steeper at low p_{T} and flatter at high p_{T}. The maximum deviation of the yield for each p_{T} bin of the unfolded spectra within the reasonable range of β is used as the systematic uncertainty. The uncertainty is largest for the unbiased jet sample with resolution parameter $R = 0.3$ in the most central collisions up to 20% at low $p_{\mathrm{T,jet}}$.

Unfolding method The spectrum obtained with the χ^2 minimization method is compared to results using the Bayesian and SVD unfolding methods. The χ^2 and SVD unfolded spectra agree within $\pm 10\%$ for all centrality classes and jet samples. The Bayesian method is only included in the estimate of the systematic uncertainties for the cases where the combinatorial jets are suppressed by selecting jets with a leading track with $p_{\mathrm{T}} > 5$ or 10 GeV/c. Without this selection, the Bayesian method was found to be unreliable: large deviations up to 50% at low $p_{\mathrm{T,jet}}$ are observed in central collisions with a resolution parameter $R = 0.3$. Such deviations are also seen in the validation studies with a heavy-ion background model where the Bayesian method did not give the correct result, unless the truth was used as the prior.

Prior The unfolding algorithm starts from a QCD inspired shape for the unfolded spectrum, the prior. The measured jet spectrum is used as a standard prior for all unfolding methods and the sensitivity to the choice of prior is evaluated by changing the shape and yield of the prior. When the prior is far from the truth (for example a uniform distribution), the χ^2 unfolding takes more iterations to converge but eventually an unfolded jet spectrum is obtained, which is statistically not significantly different from the unfolded spectrum obtained with the measured spectrum as a prior. The choice of prior has a negligible effect on the final unfolded spectrum.

2.7.2 Combinatorial jets

The effect of combinatorial jets in the sample is evaluated by changing the minimum p_{T} of the unfolded spectrum and the measured range where the unfolding is applied.

Minimum p_{T} of unfolded jet spectrum In the default analysis the unfolded spectrum starts at $p_{\mathrm{T,ch\,jet}} = 0$ GeV/c. The sensitivity of the result to very low energy (combinatorial) jets is explored by removing the first bin from the unfolding procedure, i.e. starting the unfolded spectrum at $p_{\mathrm{T,ch\,jet}} = 5$ or 10 GeV/c instead of $p_{\mathrm{T,ch\,jet}} = 0$. This removes one parameter from the χ^2 minimization. It results in an increase of the unfolded jet yield by a few percent depending on the centrality bin and jet radius.

Minimum p_{T} of measured jet spectrum Increasing the minimum measured p_{T} reduces the amount of combinatorial jets in the measured spectrum (see Fig. 1). The remaining combinatorial jets contribute to the jet yield at low p_{T} in the unfolded spectrum. The minimum p_{T} of the measured jet spectrum is varied by 10 GeV/c to a lower and higher value. With the two variations the unfolding is performed again and the resulting difference between the unfolded spectra with the default one assigned as a systematic uncertainty. This systematic uncertainty is largest at low p_{T} in the region where the $p_{\mathrm{T}}^{\mathrm{min,meas}}$ cut-off is placed. For unbiased jets in most central collisions and resolution parameter $R = 0.3$ the uncertainty at $p_{\mathrm{T,jet}} = 40$ GeV/c is 25%, while it decreases to a few percent for $p_{\mathrm{T,jet}} > 60$ GeV/c.

2.7.3 Uncertainty on background

Background fluctuation distribution: random cones and high p_{T} probe embedding The $\delta p_{\mathrm{T}}^{\mathrm{ch}}$ distribution obtained from embedding single high p_{T} tracks in measured Pb–Pb events is used as a variation to the $\delta p_{\mathrm{T}}^{\mathrm{ch}}$ distribution from random cones. The width of the background fluctuations obtained from

single-track embedding is a few 100 MeV/c larger than for the random cones. The uncertainty is taken as the difference between the unfolded jet spectrum using the $\delta p_{\rm T}^{\rm ch}$ response from single-track embedding and the response from random cones. The difference is largest at low $p_{\rm T,jet}$ (< 40 GeV/c), where $\sim 15\%$ deviation in the jet yield for the unbiased $R = 0.3$ central jet spectrum is observed.

Correction for collective flow effects in case of leading track biased jets Due to the presence of collective effects such as elliptic and triangular flow in heavy-ion collisions the background density differs from region-to-region. Jets with a high $p_{\rm T}$ leading track are preferentially found in regions with larger background density (in-plane). The subtracted background, however, is the average $p_{\rm T}$ density of the event, $\rho_{\rm ch}$, multiplied by the area of the jet. A correction for the larger background for biased jets is included in the response matrix. This correction is determined by calculating $\rho_{\rm ch}$ on the near, away side and in the region perpendicular to the leading track biased jet in an event. The correction is largest for events in the 10-30% centrality class where for $R = 0.3$ jets with a 5 GeV/c bias an overall increase of the background of 0.49 GeV/c is present. The correction for flow effects is only applied for leading track biased jet spectra since for the unbiased case, jets are selected regardless of their correlation with the event or participant plane [27].

The uncertainty on the correction for flow effects is calculated by changing the background to the lowest and highest values found in the different azimuthal regions (perpedicular and near-side regions respectively). The uncertainty on $\rho_{\rm ch}$ is 3 GeV/c for the jet sample with a 5 GeV/c leading track selection, and 2 GeV/c for a 10 GeV/c leading track requirement in central events. The systematic uncertainty on the unfolded jet spectrum for $R = 0.3$ jets with $p_{\rm T}^{\text{leading track}} > 5$ GeV/c in 10% most central collisions is 8% at $p_{\rm T,jet} = 40$ GeV/c and decreases to 4% at $p_{\rm T,jet} = 100$ GeV/c. A previous study has shown that the background fluctuations ($\delta p_{\rm T}$-distribution) are almost independent of the orientation with respect to the reaction plane [27]; this effect is negligible compared to the change in the average background.

2.7.4 Uncertainty on the detector response

The detector response has two main components: tracking efficiency and momentum resolution of which the tracking efficiency is the dominant uncertainty. The uncertainty on the tracking efficiency is estimated to be 4%, motivated by detector simulation studies with PYTHIA and HIJING events, and by varying the track selection criteria. To determine the systematic uncertainty on the result, a second response matrix is constructed from a simulation with a 4% lower efficiency and the measured Pb–Pb jet spectrum is unfolded. The difference between the nominal unfolded solution and the unfolded spectra with a modified detector response is $\sim 20\%$ at $p_{\rm T,jet} = 50$ GeV/c and decreases to $\sim 11\%$ at $p_{\rm T,jet} = 100$ GeV/c; the full difference is used as the systematic uncertainty, which corresponds to a 3–5% uncertainty on the charged jet $p_{\rm T}$.

2.7.5 Centrality determination

The relative uncertainty on the fraction of hadronic cross-section used in the Glauber fit to determine the centrality classes is 1% [19]. The contribution of this uncertainty on the jet spectrum is estimated by varying the limits of the centrality classes by $\pm 1\%$ (e.g. for the 10–30% centrality class to 9.9–29.7% and 10.1–30.3%). With the shifted limits of the centrality classes the jet spectrum is compared to the nominal jet spectrum. The uncertainty is the same for the jet spectrum with different leading track biases and increases from central to peripheral events. For the 0–10% centrality class the uncertainty is less than 1% and in the peripheral centrality class 50–80% it is $\sim 1.9\%$.

2.7.6 Total systematic uncertainty

The differential production yields are reported with their systematic uncertainties separated into two categories:

Centrality class	Resolution parameter	$R = 0.2$		$R = 0.3$	
	p_{T}-interval (GeV/c)	30–40	70–80	30–40	70–80
0–10%	Regularisation	$^{+3.4}_{-0.0}$	$^{+2.3}_{-0.3}$	$^{+9.9}_{-0.0}$	$^{+2.6}_{-6.7}$
	Unfolding method	$^{+0.0}_{-3.5}$	$^{+0.0}_{-1.1}$	$^{+0.0}_{-7.3}$	$^{+7.6}_{-0.0}$
	Minimum p_{T} unfolded	$^{+9.6}_{-0.0}$	$^{+0.3}_{-0.0}$	$^{+0.0}_{-5.9}$	$^{+0.0}_{-1.8}$
	Minimum p_{T} measured	$^{+1.7}_{-4.8}$	$^{+0.2}_{-0.3}$	$^{+0.0}_{-13}$	$^{+0.0}_{-2.1}$
	Prior	< 0.1			
	$\delta p_{\mathrm{T}}^{\mathrm{ch}}$	$^{+0.0}_{-4.9}$	$^{+0.0}_{-2.1}$	$^{+0.0}_{-27}$	$^{+0.0}_{-4.6}$
	Detector effects	± 2.7	± 5.5	± 4.6	± 5.2
	Flow bias	$^{+0.9}_{-5.8}$	$^{+0.4}_{-4.1}$	$^{+7.3}_{-5.9}$	$^{+4.8}_{-4.1}$
	Centrality determination	0.8			
	Total shape uncertainty	$^{+10}_{-7.6}$	$^{+2.4}_{-2.4}$	$^{+9.9}_{-31}$	$^{+7.6}_{-8.6}$
	Total correlated uncertainty	$^{+2.9}_{-6.4}$	$^{+5.6}_{-6.9}$	$^{+8.6}_{-7.5}$	$^{+7.1}_{-6.6}$
50–80%	Regularisation	$^{+0.0}_{-5.5}$	$^{+13}_{-4.1}$	$^{+0.1}_{-5.1}$	$^{+17}_{-2.2}$
	Unfolding method	$^{+2.1}_{-0.0}$	$^{+0.0}_{-20}$	$^{+2.3}_{-0.0}$	$^{+0.0}_{-20}$
	Minimum p_{T} unfolded	$^{+0.3}_{-0.0}$	$^{+0.1}_{-0.0}$	$^{+1.0}_{-0.0}$	$^{+0.6}_{-0.0}$
	Minimum p_{T} measured	$^{+9.3}_{-0.0}$	$^{+0.7}_{-0.4}$	$^{+7.5}_{-0.0}$	$^{+1.0}_{-0.0}$
	Prior	< 0.1			
	$\delta p_{\mathrm{T}}^{\mathrm{ch}}$	$^{+8.2}_{-0.0}$	$^{+2.4}_{-0.0}$	$^{+3.0}_{-0.0}$	$^{+2.2}_{-0.0}$
	Detector effects	± 3.3	± 6.2	± 3.3	± 3.1
	Flow bias	$^{+1.9}_{-1.9}$	$^{+0.3}_{-0.3}$	$^{+0.4}_{-7.2}$	$^{+0.3}_{-4.0}$
	Centrality determination	1.9			
	Total shape uncertainty	$^{+13}_{-5.5}$	$^{+13}_{-20}$	$^{+8.5}_{-5.1}$	$^{+17}_{-20}$
	Total correlated uncertainty	$^{+4.2}_{-4.2}$	$^{+6.5}_{-6.5}$	$^{+3.8}_{-8.2}$	$^{+3.6}_{-5.4}$

Table 3: Overview of systematic uncertainties for jet spectra with a leading track with $p_{\mathrm{T}} > 5$ GeV/c. Relative uncertainties are given in percentiles for two p_{T}-intervals and two different centrality intervals.

– **Shape uncertainty** These are uncertainties that are highly anti-correlated between parts of the spectrum: if the yield is increased in some bins, it decreases in other bins. The uncertainties from the unfolding method and regularisation, and the uncertainty on the background fluctuations (only $\delta p_{\mathrm{T}}^{\mathrm{ch}}$ uncertainty) fall into this category. The contributions are added in quadrature.

– **Correlated systematic uncertainty** These are uncertainties that result in correlated changes over the entire spectrum. The contributions to this type of uncertainty are the uncertainty on the detector response, the effect of flow in the background, and the influence of the combinatorial jets. The contributions are added in quadrature.

2.7.7 Systematic uncertainty on ratios

The following procedures are used for ratios of jet spectra:

– **Uncorrelated uncertainties** The systematic uncertainties from the unfolding method, which in-

clude regularisation and variation of $p_{\rm T}$-ranges, are not correlated from one unfolded jet spectrum to another. The contributions from these sources are added in quadrature to calculate the uncertainies on ratios.

– **Correlated uncertainties** The systematic uncertainties from the flow bias, the $\delta p_{\rm T}^{\rm ch}$-distribution, and the detector effects are highly correlated between unfolded spectra from different centrality classes, jet resolution parameters and leading track biases. The uncertainty on the tracking efficiency is similar for all centrality classes. The flow bias depends on the $p_{\rm T}$ of the leading track, jet resolution parameter, and centrality class but is correlated. As a consequence, within a ratio the correlated systematic uncertainties partially cancel.

3 Results

Jet spectra are measured with resolution parameters $R = 0.2$ and 0.3 in four centrality classes: 0–10%, 10–30%, 30–50% and 50–80%. Figure 7 shows the measured Pb–Pb jet spectra reconstructed from charged constituents with $p_{\rm T} > 0.15$ GeV/c. The jet spectra are unfolded for detector effects and background fluctuations, and corrected for the jet finding efficiency as described in the preceding sections. The upper panels show the inclusive jet spectra while for the center and lower panels the jet spectra with a leading track bias of at least 5 and 10 GeV/c are shown. The markers represent the central values of the unfolded jet spectra. It should be noted that the unfolding procedure leads to correlations between the data points, because the width of the response function is similar to the bin width: neighboring $p_{\rm T}$-bins tend to fluctuate together (correlated) while bins with some distance tend to be anti-correlated. The vertical error bars represent the statistical uncertainties. The filled and open boxes indicate the corresponding shape and correlated systematic uncertainties discussed previously.

The jet yield is given per event and normalized by the average number of nucleon-nucleon collisions $N_{\rm coll}$ corresponding to the given centrality interval. The markers shown below 20 GeV/c indicate the normalization uncertainty on the extracted values of $N_{\rm coll}$ (see Table 1). The jet yield evolves with centrality: for central collisions fewer jets are observed per $N_{\rm coll}$ than in peripheral collisions.

The left panels in Fig. 8 show the ratio between the unbiased jet spectra and jets with a leading track of at least 5 GeV/c. Although the biased spectrum is a subset of the unbiased spectrum, the statistical uncertainties are added in quadrature since the unfolding procedure introduces a point-to-point correlation between the statistical uncertainties. In the jet $p_{\rm T}$-range considered here, $p_{\rm T,ch\,jet} > 20$ GeV/c, the PYTHIA vacuum expectation from the Perugia-2011 tune [34] is that almost all jets have a constituent of at least 5 GeV/c, resulting in a ratio at unity as indicated by the PYTHIA data points. The ratio between the unbiased and 5 GeV/c biased measured Pb–Pb jet spectra is consistent in peripheral and central collisions with the vacuum expectation. No evidence of the modification of the hard jet core is observed.

The right panels in Fig. 8 show the ratio between the jet spectra with a leading track $p_{\rm T}$ of at least 10 GeV/c and 5 GeV/c as measured in central and peripheral Pb–Pb collisions compared to the same observable at particle level in PYTHIA with the Perugia-2011 tune. By selecting jets with a higher momentum for the leading jet constituent, low $p_{\rm T}$ jets with a soft fragmentation pattern are removed from the sample. The ratio increases with $p_{\rm T}$ reaching unity at $p_{\rm T,ch\,jet} = 50$ GeV/c for $R = 0.2$ jets and at $p_{\rm T,ch\,jet} = 60$ GeV/c for $R = 0.3$ jets in central and peripheral collisions. This rising trend is due to the increased fragmentation bias and is compatible with the fragmentation bias observed in PYTHIA.

Jet quenching in most central heavy-ion collisions is quantified by constructing the jet nuclear modifica-

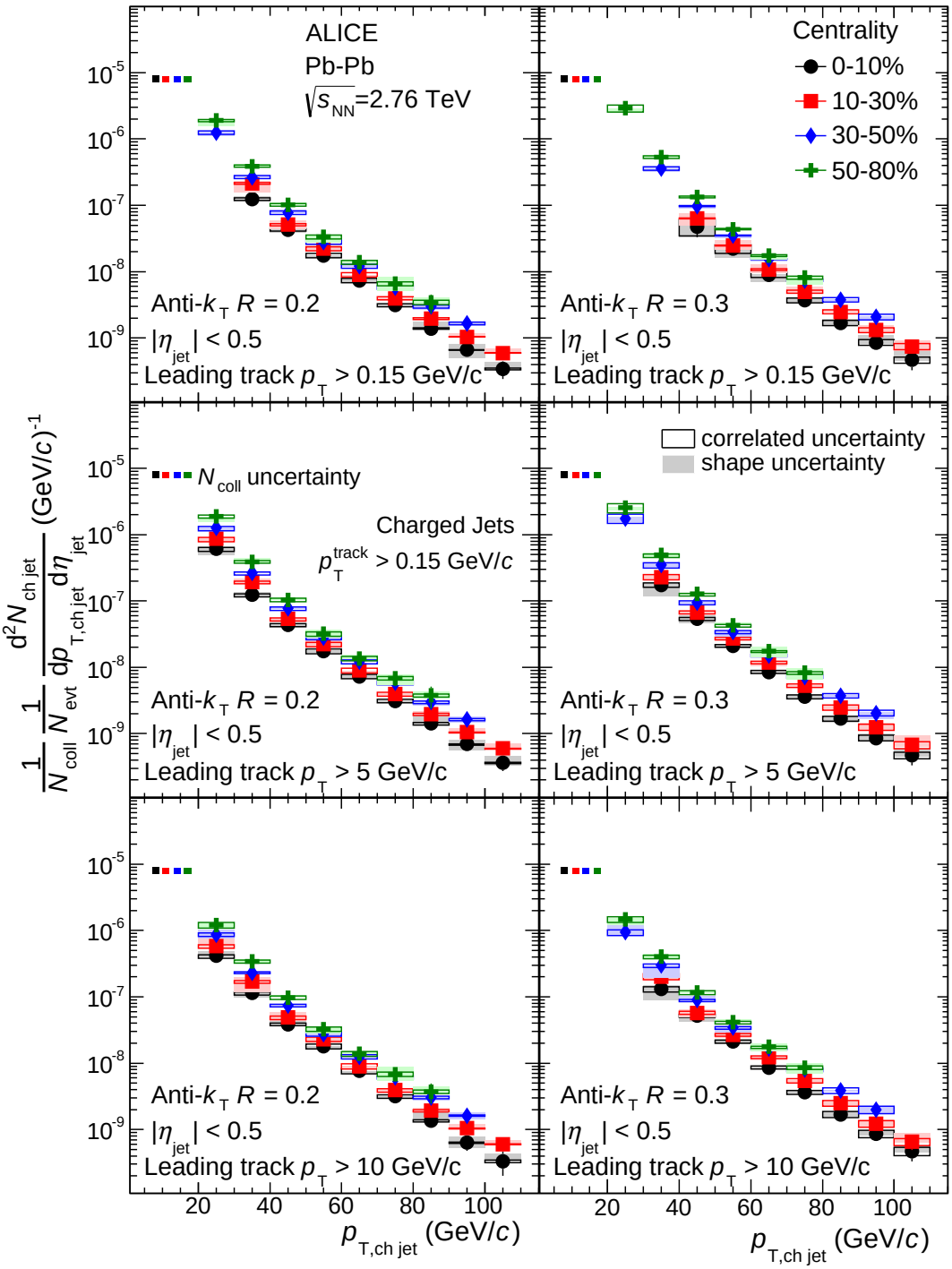

Fig. 7: Charged jet spectra, corrected for background fluctuations and detector effects, using two cone radius parameters $R = 0.2$ (left panels) and $R = 0.3$ (right panels) and different leading track selections: unbiased (top panels), $p_{\mathrm{T}}^{\text{leading track}} > 5$ GeV/c (middle panels), and $p_{\mathrm{T}}^{\text{leading track}} > 10$ GeV/c (bottom panels). The uncertainty bands at $p_{\mathrm{T,ch\,jet}} < 20\,\mathrm{GeV}/c$ indicate the normalisation uncertainty due to the scaling with $1/N_{\mathrm{coll}}$.

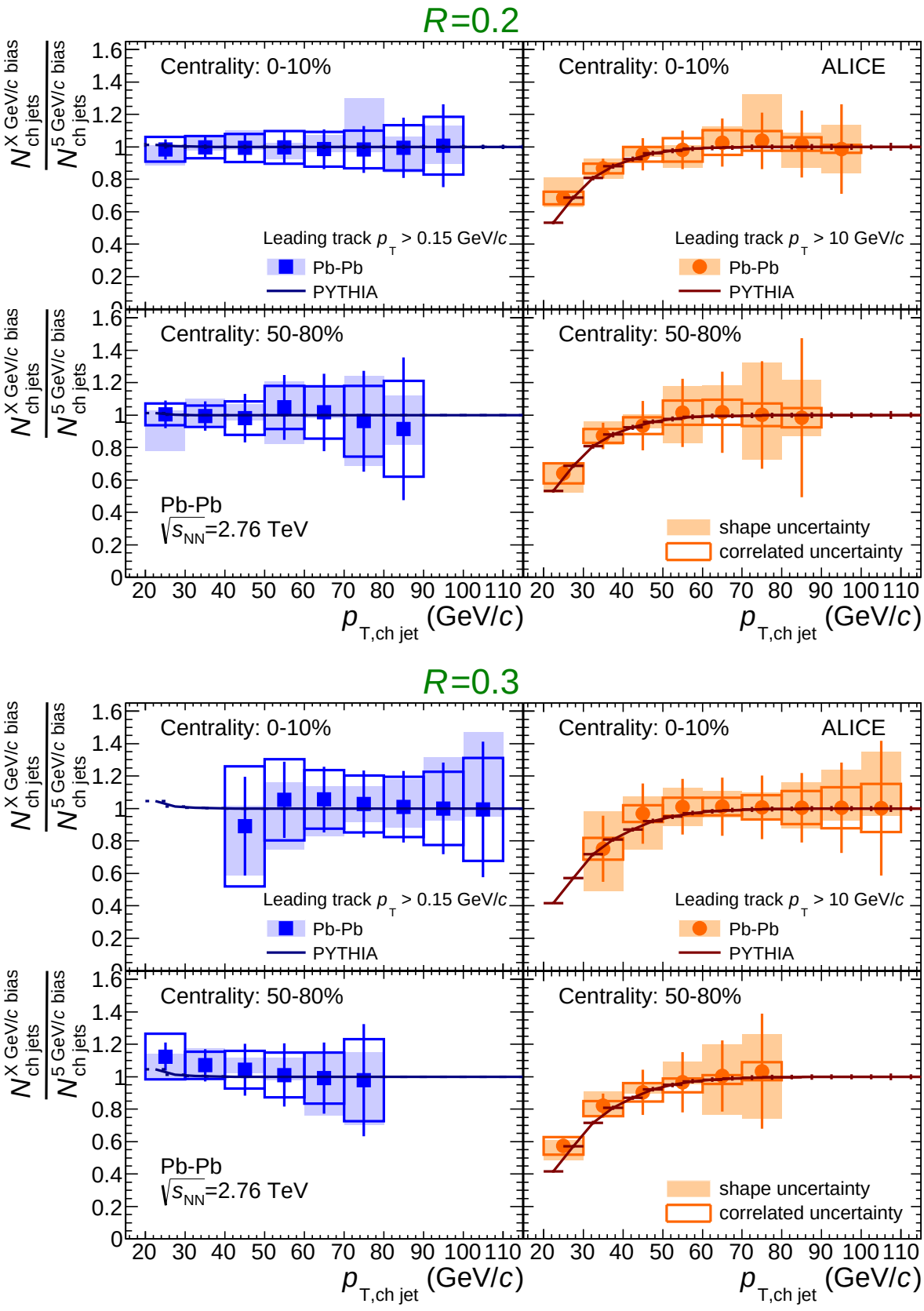

Fig. 8: Ratio of reconstructed unbiased and leading track biased jet yields for two resolution parameters (top panel: $R = 0.2$; bottom panel: $R = 0.3$). Calculations of the same ratio with the PYTHIA model (particle level) are shown for reference. Left panels: ratio of unbiased spectra to $p_{\mathrm{T}}^{\text{leading track}} > 5$ GeV/c. Right panels: ratio of spectra with $p_{\mathrm{T}}^{\text{leading track}} > 10$ GeV/c to $p_{\mathrm{T}}^{\text{leading track}} > 5$ GeV/c.

tion factor R_{CP},

$$R_{\mathrm{CP}} = \frac{\dfrac{1}{\langle T_{\mathrm{AA}} \rangle} \dfrac{1}{N_{\mathrm{evt}}} \dfrac{\mathrm{d}^2 N_{\mathrm{ch\ jet}}}{\mathrm{d}p_{\mathrm{T,ch\ jet}} \mathrm{d}\eta_{\mathrm{ch\ jet}}}\Big|_{\mathrm{central}}}{\dfrac{1}{\langle T_{\mathrm{AA}} \rangle} \dfrac{1}{N_{\mathrm{evt}}} \dfrac{\mathrm{d}^2 N_{\mathrm{ch\ jet}}}{\mathrm{d}p_{\mathrm{T,ch\ jet}} \mathrm{d}\eta_{\mathrm{ch\ jet}}}\Big|_{\mathrm{peripheral}}}, \tag{3}$$

which is the ratio of jet p_{T} spectra in central and peripheral collisions normalized by the nuclear overlap functions $\langle T_{\mathrm{AA}} \rangle$ as calculated with a Glauber model for each centrality class [19]. If the full jet energy is recovered within the cone, and in the absence of initial state effects like parton shadowing [42–44], R_{CP} is unity by construction. In that case, jet quenching would manifest itself as redistribution of the energy within the cone as compared to jet fragmentation in the vacuum. The jet suppression factor R_{CP} is shown in Fig. 9, using centrality class 50-80% as the peripheral reference. A strong jet suppression, $0.3 < R_{\mathrm{CP}} < 0.5$, is observed for 0-10% central events, while more peripheral collisions (30-50%) are less suppressed, $R_{\mathrm{CP}} \simeq 0.8$ at high $p_{\mathrm{T,ch\ jet}}$. A mild increase of R_{CP} with increasing $p_{\mathrm{T,ch\ jet}}$ is observed at low jet energies while at high $p_{\mathrm{T}} \gtrsim 50$ GeV/c the suppression is consistent with a constant. The R_{CP} does not change significantly with the resolution parameter R for the range studied ($R = 0.2$ and $R = 0.3$).

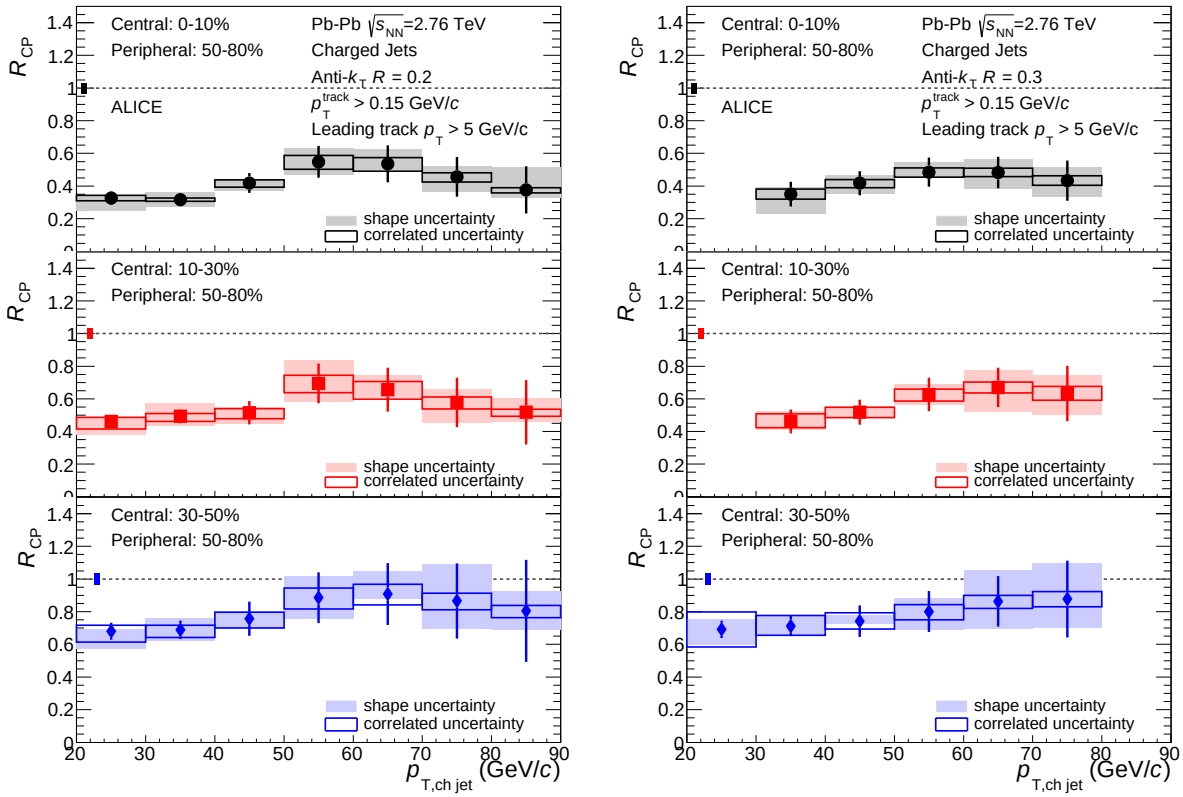

Fig. 9: Nuclear modification factor R_{CP} for charged jets with a leading charged particle with $p_{\mathrm{T}}^{\mathrm{track}} > 5$ GeV/c, with $R = 0.2$ (left panels) and $R = 0.3$ (right panels) and different centrality selections.

Figure 10 shows the jet R_{CP} at $60 < p_{\mathrm{T,ch\ jet}} < 70$ GeV/c as a function of the average number of participant nucleons corresponding to the selected centrality classes (see Table 1). A decreasing trend of the R_{CP} as a function of the number of participants is observed. Figure 10 also compares the suppression of jets with a high p_{T} track selection, and shows no evident dependence on the fragmentation pattern.

The ratio of the jet p_{T} spectra measured at different R can potentially provide information about jet structure modifications due to redistribution of energy caused by jet quenching [45,46]. Figure 11 shows the measured ratio $\sigma(R = 0.2)/\sigma(R = 0.3)$ for central and peripheral collisions. The comparison of the

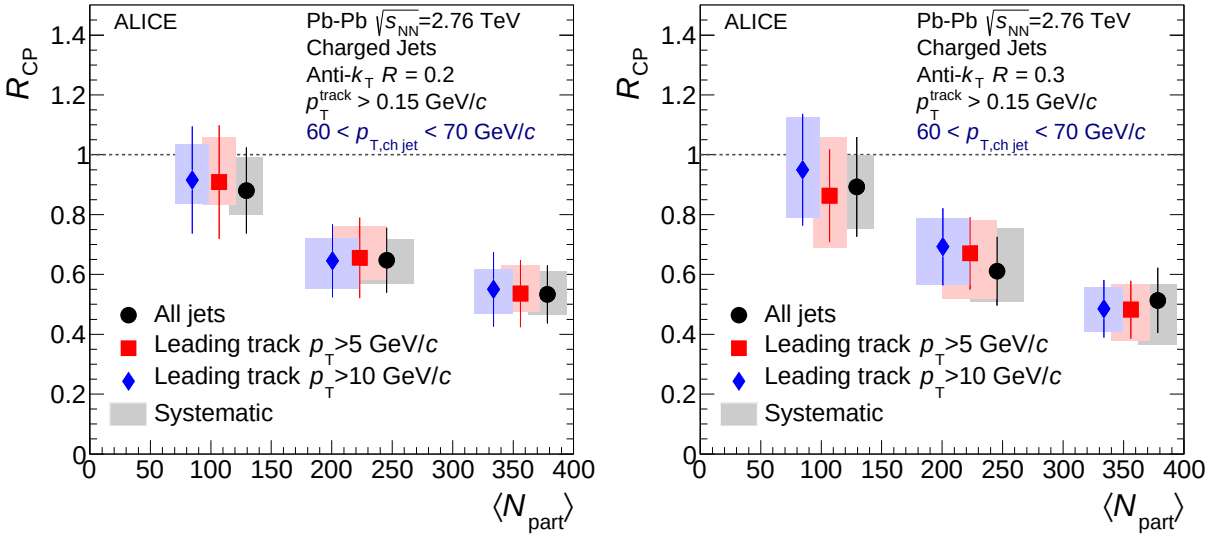

Fig. 10: $R_{\rm CP}$ for unbiased and leading track biased jets with $60 < p_{\rm T,ch\ jet} < 70$ GeV/c as a function of the average number of participants in the collision. Left panel: $R = 0.2$. Right panel: $R = 0.3$. For visibility the data points for all jets and for jets with $p_{\rm T}^{\rm track} > 10$ GeV/c are shifted to the left and right respectively.

measured ratio to the ratio obtained with PYTHIA (particle level) shows that the transverse jet shape in central and peripheral Pb–Pb collisions are consistent with jet shapes in vacuum. No sign of a modified jet structure is observed between radii of 0.2 and 0.3 within uncertainties.

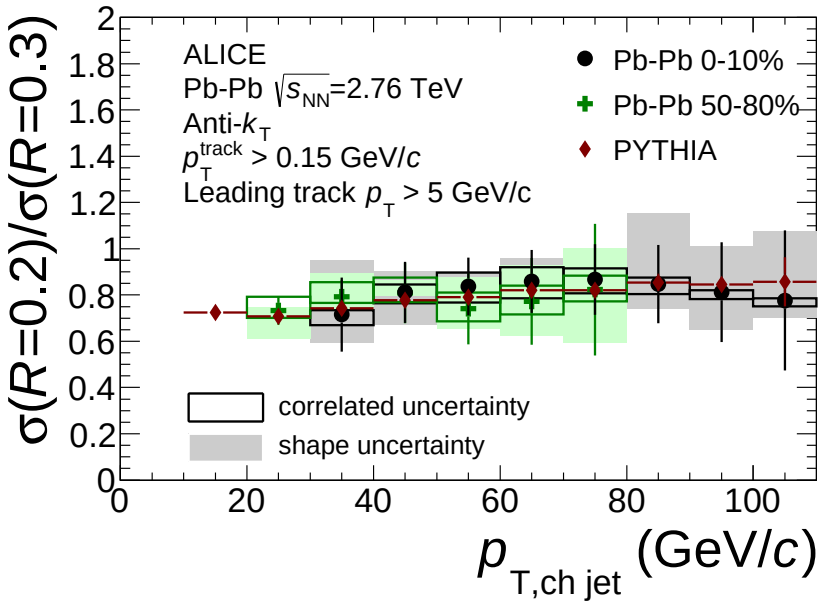

Fig. 11: Ratio of charged jet $p_{\rm T}$-spectra with radius parameter $R = 0.2$ and 0.3 and a leading charged particle $p_{\rm T}^{\rm track} > 5$ GeV/c in Pb–Pb data and simulated PYTHIA events.

4 Discussion and Conclusions

Initially, it was expected that medium interactions redistribute the momenta of jet fragments to small or moderate angles, because of kinematic effects (the momentum of the jet is large compared to the typical momenta of partons in the medium) as well as dynamics (the cross section for medium-induced radiation peaks at small angles [47]). It was therefore expected that for sufficiently large cone radii, there would be no strong suppression of jets, $R_{\mathrm{CP}} \approx 1$. The large suppression of charged jet production with $R = 0.2$ and $R = 0.3$ in central Pb–Pb collisions shown in Fig. 9, is in quantitative disagreement with these early expectations. More recently, it was found that large angle radiation is kinematically favoured for large medium density in numerical calculations [48] and in q-PYTHIA [49,50]. A number of mechanisms that may further contribute to large angle radiation have recently been discussed in the literature, such as jet broadening by medium-induced virtuality (YaJEM) [51, 52], reinteractions of the radiated gluons (also called 'frequency collimation of the radiation') [53, 54], and quantum (de-)coherence effects [55, 56].

To further explore these effects, Fig. 12 compares the jet measurement reported in this paper to the nuclear modification factor for charged hadrons measured by ALICE [57] and CMS [14] and to the calorimetric jet measurements by ATLAS [17].

Comparing the R_{CP} of jets to charged particles in Fig. 12, one would expect the suppression for jets to be smaller than for hadrons, since jet reconstruction collects multiple jet fragments into the jet cone, thus recovering some of the medium-induced fragmentation. However, it can be seen that the R_{CP} for jets is similar to that observed for single hadrons. This indicates that the momentum is redistributed to angles larger than $R = 0.3$ by interactions with the medium.

Such a strong redistribution of momentum might also be expected to lead to a significant broadening of the energy profile within the larger cone radius $R = 0.3$. The results presented in this paper, however, show that the ratio of yields for jets with $R = 0.2$ and $R = 0.3$ is similar in PYTHIA pp simulations and Pb–Pb collisions (see Fig. 11), indicating that the energy profile of the found jets is not significantly modified. In addition, Fig. 8 shows that the effect of selecting jets with a leading hadron with $p_{\mathrm{T}} > 5$ or 10 GeV/c is similar in Pb–Pb collisions and in PYTHIA pp events, which indicates that the longitudinal momentum distribution of (leading) high p_{T} tracks in jets reconstructed in Pb-Pb collisions remains

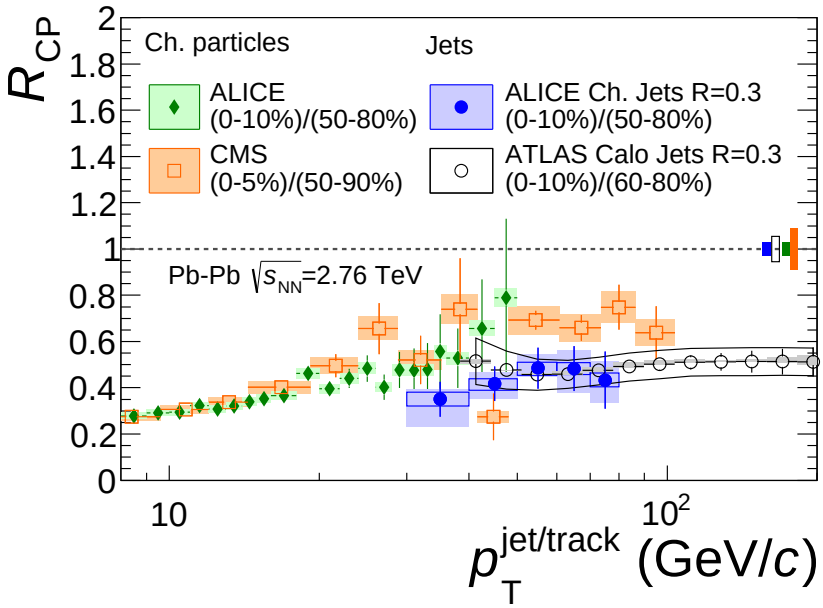

Fig. 12: Comparison to jet R_{CP} measured by ATLAS [17] and to charged particle suppression by ALICE [57] and CMS [14].

largely unmodified.

A further impression of the importance of soft radiation can be obtained by comparing the calorimetric jet measurement by ATLAS to the ALICE results in this paper. The ALICE measurement is more sensitive to low-momentum fragments due to the high tracking efficiency and good momentum resolution of charged particle tracks at low $p_{\rm T}$. The agreement between these two jet measurements in Fig. 12 suggests that the contribution of low momentum fragments to the jet energy is small. A study of PYTHIA events shows that the expected contribution of fragments with $p_{\rm T} < 1(2)$ GeV/c is 4(7)% of the jet energy at $p_{\rm T,ch\,jet} = 40$ GeV/c with cone radius $R = 0.2(0.3)$ in pp collisions. The results indicate that this contribution is also limited in Pb–Pb collisions.

The measured ratios of jet cross sections with $R = 0.2$ and $R = 0.3$ and with and without leading particle selection show that the transverse and longitudinal fragment distributions of the reconstructed jets are similar in pp (PYTHIA calculations) and Pb–Pb collisions. This 'unmodifed hard core' of the jet may be due to formation time effects (the parton leaves the medium with relatively high momentum and then fragments without further interactions) [51, 58], quantum interference effects (a group of partons with small opening angles interacts with the medium as one parton) [59], kinematics (large momentum emissions are kinematically favoured at small angles) [51] and/or selection bias effects [51, 60].

First results from the JEWEL event generator show a strong suppression of jets, in agreement with the $R_{\rm CP}$ shown in Fig. 12 [61]. However, more extensive comparisons of theoretical models to the different experimental measurements are needed to determine how well they constrain the dynamics of parton energy loss models.

In summary, we have reported measurements of charged jet spectra in Pb–Pb collisions at different centralities, using charged hadrons with $p_{\rm T} > 0.15$ GeV/c. The analysis was performed for a jet sample with a minimal fragmentation bias by introducing different $p_{\rm T}$-ranges in the unfolding procedure for the unfolded and measured spectrum. To suppress combinatorial jets from the measured population, jet spectra with a leading track selection of $p_{\rm T}^{\rm leading\ track} > 5$ and 10 GeV/c were also reported. The effect of the leading track cut at 5 GeV/c is small for the measured range $p_{\rm T,ch\,jet} > 20$ GeV/c, while for $p_{\rm T}^{\rm leading\ track} > 10$ GeV/c, the effect is sizeable, but consistent with expectations from jet fragmentation in PYTHIA events, indicating that the high-$p_{\rm T}$ fragmentation is not strongly modified by interactions with the medium. The ratio of jets reconstructed with $R = 0.2$ and $R = 0.3$ is found to be similar in central and peripheral Pb–Pb events, and similar to PYTHIA calculations, indicating no strong broadening of the radial jet profile within $R = 0.3$. The nuclear modification factor $R_{\rm CP}$ for jets is in the range 0.3–0.5, and tends to be lower at low $p_{\rm T,ch\,jet} \approx 30$ GeV/c than at high $p_{\rm T,ch\,jet} \approx 100$ GeV/c. The value of $R_{\rm CP}$ for jets is similar to charged hadrons, which suggests that interactions with the medium redistribute energy and momentum to relatively large angles with respect to the jet axis.

Acknowledgements

The ALICE collaboration would like to thank all its engineers and technicians for their invaluable contributions to the construction of the experiment and the CERN accelerator teams for the outstanding performance of the LHC complex.
The ALICE collaboration gratefully acknowledges the resources and support provided by all Grid centres and the Worldwide LHC Computing Grid (WLCG) collaboration.
The ALICE collaboration acknowledges the following funding agencies for their support in building and running the ALICE detector:
State Committee of Science, World Federation of Scientists (WFS) and Swiss Fonds Kidagan, Armenia, Conselho Nacional de Desenvolvimento Científico e Tecnológico (CNPq), Financiadora de Estudos e Projetos (FINEP), Fundação de Amparo à Pesquisa do Estado de São Paulo (FAPESP);
National Natural Science Foundation of China (NSFC), the Chinese Ministry of Education (CMOE) and

the Ministry of Science and Technology of China (MSTC);
Ministry of Education and Youth of the Czech Republic;
Danish Natural Science Research Council, the Carlsberg Foundation and the Danish National Research Foundation;
The European Research Council under the European Community's Seventh Framework Programme;
Helsinki Institute of Physics and the Academy of Finland;
French CNRS-IN2P3, the 'Region Pays de Loire', 'Region Alsace', 'Region Auvergne' and CEA, France;
German BMBF and the Helmholtz Association;
General Secretariat for Research and Technology, Ministry of Development, Greece;
Hungarian OTKA and National Office for Research and Technology (NKTH);
Department of Atomic Energy and Department of Science and Technology of the Government of India;
Istituto Nazionale di Fisica Nucleare (INFN) and Centro Fermi - Museo Storico della Fisica e Centro Studi e Ricerche "Enrico Fermi", Italy;
MEXT Grant-in-Aid for Specially Promoted Research, Japan;
Joint Institute for Nuclear Research, Dubna;
National Research Foundation of Korea (NRF);
CONACYT, DGAPA, México, ALFA-EC and the EPLANET Program (European Particle Physics Latin American Network)
Stichting voor Fundamenteel Onderzoek der Materie (FOM) and the Nederlandse Organisatie voor Wetenschappelijk Onderzoek (NWO), Netherlands;
Research Council of Norway (NFR);
Polish Ministry of Science and Higher Education;
National Science Centre, Poland;
Ministry of National Education/Institute for Atomic Physics and CNCS-UEFISCDI - Romania;
Ministry of Education and Science of Russian Federation, Russian Academy of Sciences, Russian Federal Agency of Atomic Energy, Russian Federal Agency for Science and Innovations and The Russian Foundation for Basic Research;
Ministry of Education of Slovakia;
Department of Science and Technology, South Africa;
CIEMAT, EELA, Ministerio de Economía y Competitividad (MINECO) of Spain, Xunta de Galicia (Consellería de Educación), CEADEN, Cubaenergía, Cuba, and IAEA (International Atomic Energy Agency);
Swedish Research Council (VR) and Knut & Alice Wallenberg Foundation (KAW);
Ukraine Ministry of Education and Science;
United Kingdom Science and Technology Facilities Council (STFC);
The United States Department of Energy, the United States National Science Foundation, the State of Texas, and the State of Ohio.

A χ^2 minimization unfolding method

The χ^2 minimization method minimizes the difference between the refolded and measured spectrum [38]. The refolded spectrum is the unfolded distribution convoluted with the response matrix. The χ^2 function to be minimized indicates how well the refolded distribution describes the measured spectrum:

$$\chi^2_{\rm fit} = \sum_{\rm refolded} \left(\frac{y_{\rm refolded} - y_{\rm measured}}{\sigma_{\rm measured}} \right)^2, \tag{A.1}$$

in which y is the yield of the refolded or measured distribution and $\sigma_{\rm measured}$ the statistical uncertainty on the measured distribution. The true distribution minimizes this χ^2 function but in addition also many other fluctuating solutions exist. Heavily fluctuating solutions can be damped by adding a penalty term to the χ^2 function:

$$\chi^2 = \sum_{\rm refolded} \left(\frac{y_{\rm refolded} - y_{\rm measured}}{\sigma_{\rm measured}} \right)^2 + \beta P(y_{\rm unfolded}), \tag{A.2}$$

where $y_{\rm unfolded}$ is the unfolded distribution. $\beta P(y_{\rm unfolded})$ is the penalty term which regularizes the unfolded distribution. The strength of the applied regularization is given by β and $P(y_{\rm unfolded})$ is the regularization term favoring a certain shape. The choice of the regularization function is motivated by the expected shape of the solution. For this analysis the regularization favors a local power law which is calculated using finite differences:

$$P(y_{\rm unfolded}) = \sum_{\rm unfolded} \left(\frac{{\rm d}^2 \log y_{\rm unfolded}}{{\rm d}\log p_{\rm T}^2} \right)^2. \tag{A.3}$$

Note that the exponent in the power law is not fixed and is not required to be the same over the full unfolded solution. Sensitivity of the unfolded distribution to this particular choice of regularization can be tested by varying the regularization strength β and by comparing the unfolded distribution to a solution with a different functional shape for the regularization.

In case the regularization is dominant the penalty term is of the same order or larger than the $\chi^2_{\rm fit}$ between the refolded and measured spectrum. In this case the refolded spectrum does not describe the measured spectrum and the $\chi^2_{\rm fit}$ between the refolded and measured spectrum is large.

The covariance matrix for the unfolded spectrum is calculated in the usual way, by inverting the Hessian matrix. In case the regularization is too weak or too strong, off-diagonal correlations in the Pearson coefficients extracted from the covariance matrix appear.

B The ALICE Collaboration

B. Abelev[74], J. Adam[38], D. Adamová[82], M.M. Aggarwal[86], G. Aglieri Rinella[34], M. Agnello[92,109], A.G. Agocs[132], A. Agostinelli[26], N. Agrawal[45], Z. Ahammed[128], N. Ahmad[18], A. Ahmad Masoodi[18], I. Ahmed[15], S.U. Ahn[67], S.A. Ahn[67], I. Aimo[109,92], S. Aiola[133], M. Ajaz[15], A. Akindinov[57], D. Aleksandrov[98], B. Alessandro[109], D. Alexandre[100], A. Alici[12,103], A. Alkin[3], J. Alme[36], T. Alt[40], V. Altini[31], S. Altinpinar[17], I. Altsybeev[127], C. Alves Garcia Prado[117], C. Andrei[77], A. Andronic[95], V. Anguelov[91], J. Anielski[52], T. Antičić[96], F. Antinori[106], P. Antonioli[103], L. Aphecetche[110], H. Appelshäuser[50], N. Arbor[70], S. Arcelli[26], N. Armesto[16], R. Arnaldi[109], T. Aronsson[133], I.C. Arsene[21,95], M. Arslandok[50], A. Augustinus[34], R. Averbeck[95], T.C. Awes[83], M.D. Azmi[18,88], M. Bach[40], A. Badalà[105], Y.W. Baek[41,69], S. Bagnasco[109], R. Bailhache[50], V. Bairathi[90], R. Bala[89], A. Baldisseri[14], F. Baltasar Dos Santos Pedrosa[34], J. Bán[58], R.C. Baral[60], R. Barbera[27], F. Barile[31], G.G. Barnaföldi[132], L.S. Barnby[100], V. Barret[69], J. Bartke[114], M. Basile[26], N. Bastid[69], S. Basu[128], B. Bathen[52], G. Batigne[110], B. Batyunya[65], P.C. Batzing[21], C. Baumann[50], I.G. Bearden[79], H. Beck[50], C. Bedda[92], N.K. Behera[45], I. Belikov[53], F. Bellini[26], R. Bellwied[119], E. Belmont-Moreno[63], G. Bencedi[132], S. Beole[25], I. Berceanu[77], A. Bercuci[77], Y. Berdnikov[84,ii], D. Berenyi[132], M.E. Berger[113], A.A.E. Bergognon[110], R.A. Bertens[56],

D. Berzano[25] , L. Betev[34] , A. Bhasin[89] , A.K. Bhati[86] , B. Bhattacharjee[42] , J. Bhom[124] , L. Bianchi[25] , N. Bianchi[71] , J. Bielčík[38] , J. Bielčíková[82] , A. Bilandzic[79] , S. Bjelogrlic[56] , F. Blanco[10] , D. Blau[98] , C. Blume[50] , F. Bock[73 ,91] , F.V. Boehmer[113] , A. Bogdanov[75] , H. Bøggild[79] , M. Bogolyubsky[54] , L. Boldizsár[132] , M. Bombara[39] , J. Book[50] , H. Borel[14] , A. Borissov[94 ,131] , J. Bornschein[40] , F. Bossú[64] , M. Botje[80] , E. Botta[25] , S. Böttger[49] , P. Braun-Munzinger[95] , M. Bregant[117 ,110] , T. Breitner[49] , T.A. Broker[50] , T.A. Browning[93] , M. Broz[37] , E. Bruna[109] , G.E. Bruno[31] , D. Budnikov[97] , H. Buesching[50] , S. Bufalino[109] , P. Buncic[34] , O. Busch[91] , Z. Buthelezi[64] , D. Caffarri[28] , X. Cai[7] , H. Caines[133] , A. Caliva[56] , E. Calvo Villar[101] , P. Camerini[24] , V. Canoa Roman[34] , F. Carena[34] , W. Carena[34] , F. Carminati[34] , A. Casanova Díaz[71] , J. Castillo Castellanos[14] , E.A.R. Casula[23] , V. Catanescu[77] , C. Cavicchioli[34] , C. Ceballos Sanchez[9] , J. Cepila[38] , P. Cerello[109] , B. Chang[120] , S. Chapeland[34] , J.L. Charvet[14] , S. Chattopadhyay[128] , S. Chattopadhyay[99] , M. Cherney[85] , C. Cheshkov[126] , B. Cheynis[126] , V. Chibante Barroso[34] , D.D. Chinellato[119 ,118] , P. Chochula[34] , M. Chojnacki[79] , S. Choudhury[128] , P. Christakoglou[80] , C.H. Christensen[79] , P. Christiansen[32] , T. Chujo[124] , S.U. Chung[94] , C. Cicalo[104] , L. Cifarelli[12 ,26] , F. Cindolo[103] , J. Cleymans[88] , F. Colamaria[31] , D. Colella[31] , A. Collu[23] , M. Colocci[26] , G. Conesa Balbastre[70] , Z. Conesa del Valle[48 ,34] , M.E. Connors[133] , G. Contin[24] , J.G. Contreras[11] , T.M. Cormier[83 ,131] , Y. Corrales Morales[25] , P. Cortese[30] , I. Cortés Maldonado[2] , M.R. Cosentino[73 ,117] , F. Costa[34] , P. Crochet[69] , R. Cruz Albino[11] , E. Cuautle[62] , L. Cunqueiro[71 ,34] , A. Dainese[106] , R. Dang[7] , A. Danu[61] , D. Das[99] , I. Das[48] , K. Das[99] , S. Das[4] , A. Dash[118] , S. Dash[45] , S. De[128] , H. Delagrange[110 ,i], A. Deloff[76] , E. Dénes[132] , G. D'Erasmo[31] , G.O.V. de Barros[117] , A. De Caro[12 ,29] , G. de Cataldo[102] , J. de Cuveland[40] , A. De Falco[23] , D. De Gruttola[29 ,12] , N. De Marco[109] , S. De Pasquale[29] , R. de Rooij[56] , M.A. Diaz Corchero[10] , T. Dietel[52 ,88] , R. Divià[34] , D. Di Bari[31] , S. Di Liberto[107] , A. Di Mauro[34] , P. Di Nezza[71] , Ø. Djuvsland[17] , A. Dobrin[56 ,131] , T. Dobrowolski[76] , D. Domenicis Gimenez[117] , B. Dönigus[50] , O. Dordic[21] , S. Dorheim[113] , A.K. Dubey[128] , A. Dubla[56] , L. Ducroux[126] , P. Dupieux[69] , A.K. Dutta Majumdar[99] , D. Elia[102] , H. Engel[49] , B. Erazmus[34 ,110] , H.A. Erdal[36] , D. Eschweiler[40] , B. Espagnon[48] , M. Estienne[110] , S. Esumi[124] , D. Evans[100] , S. Evdokimov[54] , G. Eyyubova[21] , D. Fabris[106] , J. Faivre[70] , D. Falchieri[26] , A. Fantoni[71] , M. Fasel[91] , D. Fehlker[17] , L. Feldkamp[52] , D. Felea[61] , A. Feliciello[109] , G. Feofilov[127] , J. Ferencei[82] , A. Fernández Téllez[2] , E.G. Ferreiro[16] , A. Ferretti[25] , A. Festanti[28] , J. Figiel[114] , M.A.S. Figueredo[117 ,121] , S. Filchagin[97] , D. Finogeev[55] , F.M. Fionda[31] , E.M. Fiore[31] , E. Floratos[87] , M. Floris[34] , S. Foertsch[64] , P. Foka[95] , S. Fokin[98] , E. Fragiacomo[108] , A. Francescon[28 ,34] , U. Frankenfeld[95] , U. Fuchs[34] , C. Furget[70] , M. Fusco Girard[29] , J.J. Gaardhøje[79] , M. Gagliardi[25] , M. Gallio[25] , D.R. Gangadharan[19 ,73] , P. Ganoti[83 ,87] , C. Garabatos[95] , E. Garcia-Solis[13] , C. Gargiulo[34] , I. Garishvili[74] , J. Gerhard[40] , M. Germain[110] , A. Gheata[34] , M. Gheata[34 ,61] , B. Ghidini[31] , P. Ghosh[128] , S.K. Ghosh[4] , P. Gianotti[71] , P. Giubellino[34] , E. Gladysz-Dziadus[114] , P. Glässel[91] , R. Gomez[11] , P. González-Zamora[10] , S. Gorbunov[40] , L. Görlich[114] , S. Gotovac[112] , L.K. Graczykowski[130] , R. Grajcarek[91] , A. Grelli[56] , A. Grigoras[34] , C. Grigoras[34] , V. Grigoriev[75] , A. Grigoryan[1] , S. Grigoryan[65] , B. Grinyov[3] , N. Grion[108] , J.F. Grosse-Oetringhaus[34] , J.-Y. Grossiord[126] , R. Grosso[34] , F. Guber[55] , R. Guernane[70] , B. Guerzoni[26] , M. Guilbaud[126] , K. Gulbrandsen[79] , H. Gulkanyan[1] , T. Gunji[123] , A. Gupta[89] , R. Gupta[89] , K. H. Khan[15] , R. Haake[52] , Ø. Haaland[17] , C. Hadjidakis[48] , M. Haiduc[61] , H. Hamagaki[123] , G. Hamar[132] , L.D. Hanratty[100] , A. Hansen[79] , J.W. Harris[133] , H. Hartmann[40] , A. Harton[13] , D. Hatzifotiadou[103] , S. Hayashi[123] , A. Hayrapetyan[34 ,1] , S.T. Heckel[50] , M. Heide[52] , H. Helstrup[36] , A. Herghelegiu[77] , G. Herrera Corral[11] , B.A. Hess[33] , K.F. Hetland[36] , B. Hicks[133] , B. Hippolyte[53] , J. Hladky[59] , P. Hristov[34] , M. Huang[17] , T.J. Humanic[19] , D. Hutter[40] , D.S. Hwang[20] , J.-C. Ianigro[126] , R. Ilkaev[97] , I. Ilkiv[76] , M. Inaba[124] , E. Incani[23] , G.M. Innocenti[25] , C. Ionita[34] , M. Ippolitov[98] , M. Irfan[18] , M. Ivanov[95] , V. Ivanov[84] , O. Ivanytskyi[3] , A. Jachołkowski[27] , C. Jahnke[117] , H.J. Jang[67] , M.A. Janik[130] , P.H.S.Y. Jayarathna[119] , S. Jena[45 ,119] , R.T. Jimenez Bustamante[62] , P.G. Jones[100] , H. Jung[41] , A. Jusko[100] , S. Kalcher[40] , P. Kalinak[58] , A. Kalweit[34] , J. Kamin[50] , J.H. Kang[134] , V. Kaplin[75] , S. Kar[128] , A. Karasu Uysal[68] , O. Karavichev[55] , T. Karavicheva[55] , E. Karpechev[55] , U. Kebschull[49] , R. Keidel[135] , B. Ketzer[35 ,113] , M.Mohisin. Khan[18 ,iii], P. Khan[99] , S.A. Khan[128] , A. Khanzadeev[84] , Y. Kharlov[54] , B. Kileng[36] , B. Kim[134] , D.W. Kim[67 ,41] , D.J. Kim[120] , J.S. Kim[41] , M. Kim[41] , M. Kim[134] , S. Kim[20] , T. Kim[134] , S. Kirsch[40] , I. Kisel[40] , S. Kiselev[57] , A. Kisiel[130] , G. Kiss[132] , J.L. Klay[6] , J. Klein[91] , C. Klein-Bösing[52] , A. Kluge[34] , M.L. Knichel[95] , A.G. Knospe[115] , C. Kobdaj[111 ,34] , M.K. Köhler[95] , T. Kollegger[40] , A. Kolojvari[127] , V. Kondratiev[127] , N. Kondratyeva[75] , A. Konevskikh[55] , V. Kovalenko[127] , M. Kowalski[114] , S. Kox[70] , G. Koyithatta Meethaleveedu[45] , J. Kral[120] , I. Králik[58] , F. Kramer[50] , A. Kravčáková[39] , M. Krelina[38] , M. Kretz[40] , M. Krivda[100 ,58] , F. Krizek[82 ,43] , M. Krus[38] , E. Kryshen[84 ,34] , M. Krzewicki[95] , V. Kučera[82] , Y. Kucheriaev[98] , T. Kugathasan[34] , C. Kuhn[53] , P.G. Kuijer[80] , I. Kulakov[50] , J. Kumar[45] , P. Kurashvili[76] , A. Kurepin[55] , A.B. Kurepin[55] , A. Kuryakin[97] , S. Kushpil[82] , V. Kushpil[82] , M.J. Kweon[91 ,47] , Y. Kwon[134] , P. Ladron de Guevara[62] , C. Lagana Fernandes[117] , I. Lakomov[48] , R. Langoy[129] , C. Lara[49] , A. Lardeux[110] , A. Lattuca[25] , S.L. La Pointe[56 ,109] , P. La Rocca[27] ,

R. Lea[24] , G.R. Lee[100] , I. Legrand[34] , J. Lehnert[50] , R.C. Lemmon[81] , M. Lenhardt[95] , V. Lenti[102] , E. Leogrande[56] , M. Leoncino[25] , I. León Monzón[116] , P. Lévai[132] , S. Li[69 ,7] , J. Lien[129 ,17] , R. Lietava[100] , S. Lindal[21] , V. Lindenstruth[40] , C. Lippmann[95] , M.A. Lisa[19] , H.M. Ljunggren[32] , D.F. Lodato[56] , P.I. Loenne[17] , V.R. Loggins[131] , V. Loginov[75] , D. Lohner[91] , C. Loizides[73] , X. Lopez[69] , E. López Torres[9] , X.-G. Lu[91] , P. Luettig[50] , M. Lunardon[28] , J. Luo[7] , G. Luparello[56] , C. Luzzi[34] , A. M. Gago[101] , P. M. Jacobs[73] , R. Ma[133] , A. Maevskaya[55] , M. Mager[34] , D.P. Mahapatra[60] , A. Maire[91 ,53] , M. Malaev[84] , I. Maldonado Cervantes[62] , L. Malinina[65 ,iv], D. Mal'Kevich[57] , P. Malzacher[95] , A. Mamonov[97] , L. Manceau[109] , V. Manko[98] , F. Manso[69] , V. Manzari[102 ,34] , M. Marchisone[69 ,25] , J. Mareš[59] , G.V. Margagliotti[24] , A. Margotti[103] , A. Marín[95] , C. Markert[34 ,115] , M. Marquard[50] , I. Martashvili[122] , N.A. Martin[95] , P. Martinengo[34] , M.I. Martínez[2] , G. Martínez García[110] , J. Martin Blanco[110] , Y. Martynov[3] , A. Mas[110] , S. Masciocchi[95] , M. Masera[25] , A. Masoni[104] , L. Massacrier[110] , A. Mastroserio[31] , A. Matyja[114] , C. Mayer[114] , J. Mazer[122] , R. Mazumder[46] , M.A. Mazzoni[107] , F. Meddi[22] , A. Menchaca-Rocha[63] , J. Mercado Pérez[91] , M. Meres[37] , Y. Miake[124] , K. Mikhaylov[57 ,65] , L. Milano[34] , J. Milosevic[21 ,v], A. Mischke[56] , A.N. Mishra[46] , D. Miśkowiec[95] , C.M. Mitu[61] , J. Mlynarz[131] , B. Mohanty[128 ,78] , L. Molnar[53] , L. Montaño Zetina[11] , E. Montes[10] , M. Morando[28] , D.A. Moreira De Godoy[117] , S. Moretto[28] , A. Morreale[120 ,110] , A. Morsch[34] , V. Muccifora[71] , E. Mudnic[112] , S. Muhuri[128] , M. Mukherjee[128] , H. Müller[34] , M.G. Munhoz[117] , S. Murray[88 ,64] , L. Musa[34] , J. Musinsky[58] , B.K. Nandi[45] , R. Nania[103] , E. Nappi[102] , C. Nattrass[122] , T.K. Nayak[128] , S. Nazarenko[97] , A. Nedosekin[57] , M. Nicassio[95] , M. Niculescu[34 ,61] , B.S. Nielsen[79] , S. Nikolaev[98] , S. Nikulin[98] , V. Nikulin[84] , B.S. Nilsen[85] , F. Noferini[12 ,103] , P. Nomokonov[65] , G. Nooren[56] , A. Nyanin[98] , A. Nyatha[45] , J. Nystrand[17] , H. Oeschler[91 ,51] , S. Oh[133] , S.K. Oh[66 ,vi,41] , A. Okatan[68] , L. Olah[132] , J. Oleniacz[130] , A.C. Oliveira Da Silva[117] , J. Onderwaater[95] , C. Oppedisano[109] , A. Ortiz Velasquez[32] , A. Oskarsson[32] , J. Otwinowski[95] , K. Oyama[91] , Y. Pachmayer[91] , M. Pachr[38] , P. Pagano[29] , G. Paić[62] , F. Painke[40] , C. Pajares[16] , S.K. Pal[128] , A. Palmeri[105] , D. Pant[45] , V. Papikyan[1] , G.S. Pappalardo[105] , W.J. Park[95] , A. Passfeld[52] , D.I. Patalakha[54] , V. Paticchio[102] , B. Paul[99] , T. Pawlak[130] , T. Peitzmann[56] , H. Pereira Da Costa[14] , E. Pereira De Oliveira Filho[117] , D. Peresunko[98] , C.E. Pérez Lara[80] , W. Peryt[130 ,i], A. Pesci[103] , Y. Pestov[5] , V. Petráček[38] , M. Petran[38] , M. Petris[77] , M. Petrovici[77] , C. Petta[27] , S. Piano[108] , M. Pikna[37] , P. Pillot[110] , O. Pinazza[34 ,103] , L. Pinsky[119] , D.B. Piyarathna[119] , M. Płoskoń[73] , M. Planinic[96 ,125] , J. Pluta[130] , S. Pochybova[132] , P.L.M. Podesta-Lerma[116] , M.G. Poghosyan[34 ,85] , E.H.O. Pohjoisaho[43] , B. Polichtchouk[54] , N. Poljak[96 ,125] , A. Pop[77] , S. Porteboeuf-Houssais[69] , J. Porter[73] , V. Pospisil[38] , B. Potukuchi[89] , S.K. Prasad[131 ,4] , R. Preghenella[103 ,12] , F. Prino[109] , C.A. Pruneau[131] , I. Pshenichnov[55] , G. Puddu[23] , P. Pujahari[131 ,45] , V. Punin[97] , J. Putschke[131] , H. Qvigstad[21] , A. Rachevski[108] , S. Raha[4] , J. Rak[120] , A. Rakotozafindrabe[14] , L. Ramello[30] , R. Raniwala[90] , S. Raniwala[90] , S.S. Räsänen[43] , B.T. Rascanu[50] , D. Rathee[86] , A.W. Rauf[15] , V. Razazi[23] , K.F. Read[122] , J.S. Real[70] , K. Redlich[76 ,vii], R.J. Reed[133] , A. Rehman[17] , P. Reichelt[50] , M. Reicher[56] , F. Reidt[34] , R. Renfordt[50] , A.R. Reolon[71] , A. Reshetin[55] , F. Rettig[40] , J.-P. Revol[34] , K. Reygers[91] , V. Riabov[84] , R.A. Ricci[72] , T. Richert[32] , M. Richter[21] , P. Riedler[34] , W. Riegler[34] , F. Riggi[27] , A. Rivetti[109] , E. Rocco[56] , M. Rodríguez Cahuantzi[2] , A. Rodriguez Manso[80] , K. Røed[21] , E. Rogochaya[65] , S. Rohni[89] , D. Rohr[40] , D. Röhrich[17] , R. Romita[121 ,81] , F. Ronchetti[71] , L. Ronflette[110] , P. Rosnet[69] , S. Rossegger[34] , A. Rossi[34] , A. Roy[46] , C. Roy[53] , P. Roy[99] , A.J. Rubio Montero[10] , R. Rui[24] , R. Russo[25] , E. Ryabinkin[98] , Y. Ryabov[84] , A. Rybicki[114] , S. Sadovsky[54] , K. Šafařík[34] , B. Sahlmuller[50] , R. Sahoo[46] , P.K. Sahu[60] , J. Saini[128] , C.A. Salgado[16] , J. Salzwedel[19] , S. Sambyal[89] , V. Samsonov[84] , X. Sanchez Castro[53 ,62] , F.J. Sánchez Rodríguez[116] , L. Šándor[58] , A. Sandoval[63] , M. Sano[124] , G. Santagati[27] , D. Sarkar[128] , E. Scapparone[103] , F. Scarlassara[28] , R.P. Scharenberg[93] , C. Schiaua[77] , R. Schicker[91] , C. Schmidt[95] , H.R. Schmidt[33] , S. Schuchmann[50] , J. Schukraft[34] , M. Schulc[38] , T. Schuster[133] , Y. Schutz[34 ,110] , K. Schwarz[95] , K. Schweda[95] , G. Scioli[26] , E. Scomparin[109] , P.A. Scott[100] , R. Scott[122] , G. Segato[28] , J.E. Seger[85] , I. Selyuzhenkov[95] , J. Seo[94] , E. Serradilla[10 ,63] , A. Sevcenco[61] , A. Shabetai[110] , G. Shabratova[65] , R. Shahoyan[34] , A. Shangaraev[54] , N. Sharma[122 ,60] , S. Sharma[89] , K. Shigaki[44] , K. Shtejer[25] , Y. Sibiriak[98] , S. Siddhanta[104] , T. Siemiarczuk[76] , D. Silvermyr[83] , C. Silvestre[70] , G. Simatovic[125] , R. Singaraju[128] , R. Singh[89] , S. Singha[78 ,128] , V. Singhal[128] , B.C. Sinha[128] , T. Sinha[99] , B. Sitar[37] , M. Sitta[30] , T.B. Skaali[21] , K. Skjerdal[17] , R. Smakal[38] , N. Smirnov[133] , R.J.M. Snellings[56] , C. Søgaard[32] , R. Soltz[74] , J. Song[94] , M. Song[134] , F. Soramel[28] , S. Sorensen[122] , M. Spacek[38] , I. Sputowska[114] , M. Spyropoulou-Stassinaki[87] , B.K. Srivastava[93] , J. Stachel[91] , I. Stan[61] , G. Stefanek[76] , M. Steinpreis[19] , E. Stenlund[32] , G. Steyn[64] , J.H. Stiller[91] , D. Stocco[110] , M. Stolpovskiy[54] , P. Strmen[37] , A.A.P. Suaide[117] , M.A. Subieta Vasquez[25] , T. Sugitate[44] , C. Suire[48] , M. Suleymanov[15] , R. Sultanov[57] , M. Šumbera[82] , T. Susa[96] , T.J.M. Symons[73] , A. Szanto de Toledo[117] , I. Szarka[37] , A. Szczepankiewicz[34] , M. Szymanski[130] , J. Takahashi[118] , M.A. Tangaro[31] , J.D. Tapia Takaki[48 ,viii], A. Tarantola Peloni[50] , A. Tarazona Martinez[34] , A. Tauro[34] , G. Tejeda Muñoz[2] , A. Telesca[34] , C. Terrevoli[31] , A. Ter Minasyan[98 ,75] , J. Thäder[95] , D. Thomas[56] ,

R. Tieulent[126] , A.R. Timmins[119] , A. Toia[106 ,50] , H. Torii[123] , V. Trubnikov[3] , W.H. Trzaska[120] , T. Tsuji[123] , A. Tumkin[97] , R. Turrisi[106] , T.S. Tveter[21] , J. Ulery[50] , K. Ullaland[17] , J. Ulrich[49] , A. Uras[126] , G.L. Usai[23] , M. Vajzer[82] , M. Vala[58 ,65] , L. Valencia Palomo[69 ,48] , S. Vallero[25 ,91] , P. Vande Vyvre[34] , L. Vannucci[72] , J.W. Van Hoorne[34] , M. van Leeuwen[56] , A. Vargas[2] , R. Varma[45] , M. Vasileiou[87] , A. Vasiliev[98] , V. Vechernin[127] , M. Veldhoen[56] , M. Venaruzzo[24] , E. Vercellin[25] , S. Vergara Limón[2] , R. Vernet[8] , M. Verweij[131] , L. Vickovic[112] , G. Viesti[28] , J. Viinikainen[120] , Z. Vilakazi[64] , O. Villalobos Baillie[100] , A. Vinogradov[98] , L. Vinogradov[127] , Y. Vinogradov[97] , T. Virgili[29] , Y.P. Viyogi[128] , A. Vodopyanov[65] , M.A. Völkl[91] , K. Voloshin[57] , S.A. Voloshin[131] , G. Volpe[34] , B. von Haller[34] , I. Vorobyev[127] , D. Vranic[95 ,34] , J. Vrláková[39] , B. Vulpescu[69] , A. Vyushin[97] , B. Wagner[17] , J. Wagner[95] , V. Wagner[38] , M. Wang[7 ,110] , Y. Wang[91] , D. Watanabe[124] , M. Weber[119] , J.P. Wessels[52] , U. Westerhoff[52] , J. Wiechula[33] , J. Wikne[21] , M. Wilde[52] , G. Wilk[76] , J. Wilkinson[91] , M.C.S. Williams[103] , B. Windelband[91] , M. Winn[91] , C. Xiang[7] , C.G. Yaldo[131] , Y. Yamaguchi[123] , H. Yang[14 ,56] , P. Yang[7] , S. Yang[17] , S. Yano[44] , S. Yasnopolskiy[98] , J. Yi[94] , Z. Yin[7] , I.-K. Yoo[94] , I. Yushmanov[98] , V. Zaccolo[79] , C. Zach[38] , A. Zaman[15] , C. Zampolli[103] , S. Zaporozhets[65] , A. Zarochentsev[127] , P. Závada[59] , N. Zaviyalov[97] , H. Zbroszczyk[130] , I.S. Zgura[61] , M. Zhalov[84] , F. Zhang[7] , H. Zhang[7] , X. Zhang[69 ,7 ,73] , Y. Zhang[7] , C. Zhao[21] , D. Zhou[7] , F. Zhou[7] , Y. Zhou[56] , H. Zhu[7] , J. Zhu[7] , J. Zhu[7] , X. Zhu[7] , A. Zichichi[12 ,26] , A. Zimmermann[91] , M.B. Zimmermann[34 ,52] , G. Zinovjev[3] , Y. Zoccarato[126] , M. Zynovyev[3] , M. Zyzak[50]

Affiliation notes

[i] Deceased
[ii] Also at: St-Petersburg State Polytechnical University
[iii] Also at: Department of Applied Physics, Aligarh Muslim University, Aligarh, India
[iv] Also at: M.V. Lomonosov Moscow State University, D.V. Skobeltsyn Institute of Nuclear Physics, Moscow, Russia
[v] Also at: University of Belgrade, Faculty of Physics and ”Vinča” Institute of Nuclear Sciences, Belgrade, Serbia
[vi] Permanent address: Konkuk University, Seoul, Korea
[vii] Also at: Institute of Theoretical Physics, University of Wroclaw, Wroclaw, Poland
[viii] Also at: the University of Kansas, Lawrence, KS, United States

Collaboration Institutes

[1] A.I. Alikhanyan National Science Laboratory (Yerevan Physics Institute) Foundation, Yerevan, Armenia
[2] Benemérita Universidad Autónoma de Puebla, Puebla, Mexico
[3] Bogolyubov Institute for Theoretical Physics, Kiev, Ukraine
[4] Bose Institute, Department of Physics and Centre for Astroparticle Physics and Space Science (CAPSS), Kolkata, India
[5] Budker Institute for Nuclear Physics, Novosibirsk, Russia
[6] California Polytechnic State University, San Luis Obispo, CA, United States
[7] Central China Normal University, Wuhan, China
[8] Centre de Calcul de l’IN2P3, Villeurbanne, France
[9] Centro de Aplicaciones Tecnológicas y Desarrollo Nuclear (CEADEN), Havana, Cuba
[10] Centro de Investigaciones Energéticas Medioambientales y Tecnológicas (CIEMAT), Madrid, Spain
[11] Centro de Investigación y de Estudios Avanzados (CINVESTAV), Mexico City and Mérida, Mexico
[12] Centro Fermi - Museo Storico della Fisica e Centro Studi e Ricerche “Enrico Fermi”, Rome, Italy
[13] Chicago State University, Chicago, USA
[14] Commissariat à l’Energie Atomique, IRFU, Saclay, France
[15] COMSATS Institute of Information Technology (CIIT), Islamabad, Pakistan
[16] Departamento de Física de Partículas and IGFAE, Universidad de Santiago de Compostela, Santiago de Compostela, Spain
[17] Department of Physics and Technology, University of Bergen, Bergen, Norway
[18] Department of Physics, Aligarh Muslim University, Aligarh, India
[19] Department of Physics, Ohio State University, Columbus, OH, United States
[20] Department of Physics, Sejong University, Seoul, South Korea
[21] Department of Physics, University of Oslo, Oslo, Norway
[22] Dipartimento di Fisica dell’Università ’La Sapienza’ and Sezione INFN Rome

[23] Dipartimento di Fisica dell'Università and Sezione INFN, Cagliari, Italy
[24] Dipartimento di Fisica dell'Università and Sezione INFN, Trieste, Italy
[25] Dipartimento di Fisica dell'Università and Sezione INFN, Turin, Italy
[26] Dipartimento di Fisica e Astronomia dell'Università and Sezione INFN, Bologna, Italy
[27] Dipartimento di Fisica e Astronomia dell'Università and Sezione INFN, Catania, Italy
[28] Dipartimento di Fisica e Astronomia dell'Università and Sezione INFN, Padova, Italy
[29] Dipartimento di Fisica 'E.R. Caianiello' dell'Università and Gruppo Collegato INFN, Salerno, Italy
[30] Dipartimento di Scienze e Innovazione Tecnologica dell'Università del Piemonte Orientale and Gruppo Collegato INFN, Alessandria, Italy
[31] Dipartimento Interateneo di Fisica 'M. Merlin' and Sezione INFN, Bari, Italy
[32] Division of Experimental High Energy Physics, University of Lund, Lund, Sweden
[33] Eberhard Karls Universität Tübingen, Tübingen, Germany
[34] European Organization for Nuclear Research (CERN), Geneva, Switzerland
[35] Excellence Cluster Universe, Technische Universität München, Munich, Germany
[36] Faculty of Engineering, Bergen University College, Bergen, Norway
[37] Faculty of Mathematics, Physics and Informatics, Comenius University, Bratislava, Slovakia
[38] Faculty of Nuclear Sciences and Physical Engineering, Czech Technical University in Prague, Prague, Czech Republic
[39] Faculty of Science, P.J. Šafárik University, Košice, Slovakia
[40] Frankfurt Institute for Advanced Studies, Johann Wolfgang Goethe-Universität Frankfurt, Frankfurt, Germany
[41] Gangneung-Wonju National University, Gangneung, South Korea
[42] Gauhati University, Department of Physics, Guwahati, India
[43] Helsinki Institute of Physics (HIP), Helsinki, Finland
[44] Hiroshima University, Hiroshima, Japan
[45] Indian Institute of Technology Bombay (IIT), Mumbai, India
[46] Indian Institute of Technology Indore, Indore (IITI), India
[47] Inha University, College of Natural Sciences
[48] Institut de Physique Nucleaire d'Orsay (IPNO), Universite Paris-Sud, CNRS-IN2P3, Orsay, France
[49] Institut für Informatik, Johann Wolfgang Goethe-Universität Frankfurt, Frankfurt, Germany
[50] Institut für Kernphysik, Johann Wolfgang Goethe-Universität Frankfurt, Frankfurt, Germany
[51] Institut für Kernphysik, Technische Universität Darmstadt, Darmstadt, Germany
[52] Institut für Kernphysik, Westfälische Wilhelms-Universität Münster, Münster, Germany
[53] Institut Pluridisciplinaire Hubert Curien (IPHC), Université de Strasbourg, CNRS-IN2P3, Strasbourg, France
[54] Institute for High Energy Physics, Protvino, Russia
[55] Institute for Nuclear Research, Academy of Sciences, Moscow, Russia
[56] Institute for Subatomic Physics of Utrecht University, Utrecht, Netherlands
[57] Institute for Theoretical and Experimental Physics, Moscow, Russia
[58] Institute of Experimental Physics, Slovak Academy of Sciences, Košice, Slovakia
[59] Institute of Physics, Academy of Sciences of the Czech Republic, Prague, Czech Republic
[60] Institute of Physics, Bhubaneswar, India
[61] Institute of Space Science (ISS), Bucharest, Romania
[62] Instituto de Ciencias Nucleares, Universidad Nacional Autónoma de México, Mexico City, Mexico
[63] Instituto de Física, Universidad Nacional Autónoma de México, Mexico City, Mexico
[64] iThemba LABS, National Research Foundation, Somerset West, South Africa
[65] Joint Institute for Nuclear Research (JINR), Dubna, Russia
[66] Konkuk University
[67] Korea Institute of Science and Technology Information, Daejeon, South Korea
[68] KTO Karatay University, Konya, Turkey
[69] Laboratoire de Physique Corpusculaire (LPC), Clermont Université, Université Blaise Pascal, CNRS–IN2P3, Clermont-Ferrand, France
[70] Laboratoire de Physique Subatomique et de Cosmologie (LPSC), Université Joseph Fourier, CNRS-IN2P3, Institut Polytechnique de Grenoble, Grenoble, France
[71] Laboratori Nazionali di Frascati, INFN, Frascati, Italy
[72] Laboratori Nazionali di Legnaro, INFN, Legnaro, Italy

[73] Lawrence Berkeley National Laboratory, Berkeley, CA, United States
[74] Lawrence Livermore National Laboratory, Livermore, CA, United States
[75] Moscow Engineering Physics Institute, Moscow, Russia
[76] National Centre for Nuclear Studies, Warsaw, Poland
[77] National Institute for Physics and Nuclear Engineering, Bucharest, Romania
[78] National Institute of Science Education and Research, Bhubaneswar, India
[79] Niels Bohr Institute, University of Copenhagen, Copenhagen, Denmark
[80] Nikhef, National Institute for Subatomic Physics, Amsterdam, Netherlands
[81] Nuclear Physics Group, STFC Daresbury Laboratory, Daresbury, United Kingdom
[82] Nuclear Physics Institute, Academy of Sciences of the Czech Republic, Řež u Prahy, Czech Republic
[83] Oak Ridge National Laboratory, Oak Ridge, TN, United States
[84] Petersburg Nuclear Physics Institute, Gatchina, Russia
[85] Physics Department, Creighton University, Omaha, NE, United States
[86] Physics Department, Panjab University, Chandigarh, India
[87] Physics Department, University of Athens, Athens, Greece
[88] Physics Department, University of Cape Town, Cape Town, South Africa
[89] Physics Department, University of Jammu, Jammu, India
[90] Physics Department, University of Rajasthan, Jaipur, India
[91] Physikalisches Institut, Ruprecht-Karls-Universität Heidelberg, Heidelberg, Germany
[92] Politecnico di Torino, Turin, Italy
[93] Purdue University, West Lafayette, IN, United States
[94] Pusan National University, Pusan, South Korea
[95] Research Division and ExtreMe Matter Institute EMMI, GSI Helmholtzzentrum für Schwerionenforschung, Darmstadt, Germany
[96] Rudjer Bošković Institute, Zagreb, Croatia
[97] Russian Federal Nuclear Center (VNIIEF), Sarov, Russia
[98] Russian Research Centre Kurchatov Institute, Moscow, Russia
[99] Saha Institute of Nuclear Physics, Kolkata, India
[100] School of Physics and Astronomy, University of Birmingham, Birmingham, United Kingdom
[101] Sección Física, Departamento de Ciencias, Pontificia Universidad Católica del Perú, Lima, Peru
[102] Sezione INFN, Bari, Italy
[103] Sezione INFN, Bologna, Italy
[104] Sezione INFN, Cagliari, Italy
[105] Sezione INFN, Catania, Italy
[106] Sezione INFN, Padova, Italy
[107] Sezione INFN, Rome, Italy
[108] Sezione INFN, Trieste, Italy
[109] Sezione INFN, Turin, Italy
[110] SUBATECH, Ecole des Mines de Nantes, Université de Nantes, CNRS-IN2P3, Nantes, France
[111] Suranaree University of Technology, Nakhon Ratchasima, Thailand
[112] Technical University of Split FESB, Split, Croatia
[113] Technische Universität München, Munich, Germany
[114] The Henryk Niewodniczanski Institute of Nuclear Physics, Polish Academy of Sciences, Cracow, Poland
[115] The University of Texas at Austin, Physics Department, Austin, TX, USA
[116] Universidad Autónoma de Sinaloa, Culiacán, Mexico
[117] Universidade de São Paulo (USP), São Paulo, Brazil
[118] Universidade Estadual de Campinas (UNICAMP), Campinas, Brazil
[119] University of Houston, Houston, TX, United States
[120] University of Jyväskylä, Jyväskylä, Finland
[121] University of Liverpool, Liverpool, United Kingdom
[122] University of Tennessee, Knoxville, TN, United States
[123] University of Tokyo, Tokyo, Japan
[124] University of Tsukuba, Tsukuba, Japan
[125] University of Zagreb, Zagreb, Croatia
[126] Université de Lyon, Université Lyon 1, CNRS/IN2P3, IPN-Lyon, Villeurbanne, France
[127] V. Fock Institute for Physics, St. Petersburg State University, St. Petersburg, Russia

[128] Variable Energy Cyclotron Centre, Kolkata, India
[129] Vestfold University College, Tonsberg, Norway
[130] Warsaw University of Technology, Warsaw, Poland
[131] Wayne State University, Detroit, MI, United States
[132] Wigner Research Centre for Physics, Hungarian Academy of Sciences, Budapest, Hungary
[133] Yale University, New Haven, CT, United States
[134] Yonsei University, Seoul, South Korea
[135] Zentrum für Technologietransfer und Telekommunikation (ZTT), Fachhochschule Worms, Worms, Germany

References

[1] F. Karsch, E. Laermann, Thermodynamics and in-medium hadron properties from lattice QCD, in: R. C. Hwa (Ed.), Quark-Gluon Plasma 3, World Scientific, 2003, pp. 1–59. arXiv:hep-lat/0305025.

[2] A. Bazavov, et al., The chiral and deconfinement aspects of the QCD transition, Phys. Rev. D85 (2012) 054503. arXiv:1111.1710.

[3] M. Gyulassy, M. Plumer, Jet quenching in dense matter, Phys.Lett. B243 432–438.

[4] R. Baier, Y. L. Dokshitzer, S. Peigne, D. Schiff, Induced gluon radiation in a QCD medium, Phys.Lett. B345 277–286.

[5] K. Adcox, et al., Suppression of hadrons with large transverse momentum in central Au+Au collisions at $\sqrt{s_{NN}}$ = 130-GeV, Phys.Rev.Lett. 88 022301.

[6] S. S. Adler, et al., Suppressed π^0 production at large transverse momentum in central Au + Au collisions at $\sqrt{s_{NN}}$ = 200 GeV, Phys. Rev. Lett. 91 (2003) 072301.

[7] J. Adams, et al., Transverse Momentum and Collision Energy Dependence of High p_T Hadron Suppression in Au+Au Collisions at Ultrarelativistic Energies, Phys. Rev. Lett. 91 (2003) 172302. arXiv:nucl-ex/0305015.

[8] J. e. a. Adams, Evidence from $d+$Au measurements for final-state suppression of high-p_T hadrons in Au$+$Au collisions at rhic, Phys. Rev. Lett. 91 (2003) 072304.

[9] I. Arsene, et al., Transverse momentum spectra in Au+Au and d+Au collisions at s**(1/2) = 200-GeV and the pseudorapidity dependence of high p(T) suppression, Phys.Rev.Lett. 91 (2003) 072305. arXiv:nucl-ex/0307003, doi:10.1103/PhysRevLett.91.072305.

[10] B. Back, et al., Charged hadron transverse momentum distributions in au + au collisions at (S(NN))**(1/2) = 200-GeV, Phys.Lett. B578 (2004) 297–303. arXiv:nucl-ex/0302015, doi:10.1016/j.physletb.2003.10.101.

[11] K. Aamodt, et al., Suppression of charged particle production at large transverse momentum in central Pb–Pb collisions at $\sqrt{s_{NN}}$ = 2.76 TeV , Physics Letters B 696 (12) (2011) 30 – 39.

[12] K. Aamodt, et al., Particle-yield modification in jet-like azimuthal di-hadron correlations in Pb-Pb collisions at $\sqrt{s_{NN}}$ = 2.76 TeV, Phys.Rev.Lett. 108 (2012) 092301. arXiv:1110.0121, doi:10.1103/PhysRevLett.108.092301.

[13] Measurement of the charged particle spectra in PbPb collisions at $\sqrt{s_{NN}}$=2.76 TeV with the ATLAS detector at the LHC.

[14] S. Chatrchyan, et al., Study of high-pT charged particle suppression in PbPb compared to pp collisions at $\sqrt{s_{NN}} = 2.76$ TeV, Eur.Phys.J. C72 1945.

[15] G. Aad, et al., Observation of a Centrality-Dependent Dijet Asymmetry in Lead-Lead Collisions at $\sqrt{s_{NN}}$= 2.76 TeV with the ATLAS Detector at the LHC, Phys.Rev.Lett. 105 (2010) 252303. arXiv:1011.6182.

[16] S. Chatrchyan, et al., Jet momentum dependence of jet quenching in Pb–Pb collisions at $\sqrt{s_{NN}} = 2.76$ TeV, Phys.Lett. B712 176–197.

[17] G. Aad, et al., Measurement of the jet radius and transverse momentum dependence of inclusive jet suppression in lead-lead collisions at $\sqrt{s_{NN}} = 2.76$ TeV with the ATLAS detector, Phys.Lett. B719 220–241.

[18] K. Aamodt, et al.

[19] B. Abelev, et al., Centrality determination of Pb-Pb collisions at $\sqrt{s_{NN}}$ = 2.76 TeV with ALICE arXiv:1301.4361.

[20] J. Alme, Y. Andres, H. Appelshauser, S. Bablok, N. Bialas, et al., The ALICE TPC, a large 3-dimensional tracking device with fast readout for ultra-high multiplicity events, Nucl.Instrum.Meth. A622 (2010) 316–367. arXiv:1001.1950, doi:10.1016/j.nima.2010.04.042.

[21] K. Aamodt, et al., Alignment of the ALICE Inner Tracking System with cosmic-ray tracks, JINST 5 (2010) P03003. arXiv:1001.0502, doi:10.1088/1748-0221/5/03/P03003.

[22] M. Cacciari, G. P. Salam, G. Soyez, FastJet User Manual, Eur.Phys.J. C72 1896.

[23] M. Cacciari, G. P. Salam, Dispelling the n^3 myth for the kt jet-finder, Phys.Lett.B 641 (2006) 57–61. arXiv:hep-ph/0512210.

[24] M. Cacciari, G. P. Salam, G. Soyez, The catchment area of jets, JHEP 04 (2008) 005. arXiv:0802.1188.

[25] M. Cacciari, G. P. Salam, Pileup subtraction using jet areas, Phys.Lett.B 659 (2008) 119–126. arXiv:0707.1378.

[26] M. Cacciari, J. Rojo, G. P. Salam, G. Soyez, Jet reconstruction in heavy ion collisions, Eur.Phys.J.C 71 (2010) 1539. arXiv:1010.1759.

[27] B. Abelev, et al., Measurement of Event Background Fluctuations for Charged Particle Jet Reconstruction in Pb-Pb collisions at $\sqrt{s_{NN}} = 2.76$ TeV, JHEP 1203 053.

[28] J. W. Monk, C. Oropeza-Barrera, The HBOM Method for Unfolding Detector Effects, Nucl.Instrum.Meth. A701 17–24.

[29] G. de Barros, B. Fenton-Olsen, P. Jacobs, M. Ploskon, Data-driven analysis methods for the measurement of reconstructed jets in heavyion collisions at RHIC and LHC arXiv:1208.1518.

[30] M. Cacciari, J. Rojo, G. P. Salam, G. Soyez, Jet Reconstruction in Heavy Ion Collisions, Eur.Phys.J. C71 1539.

[31] T. Sjostrand, S. Mrenna, P. Skands, PYTHIA 6.4 physics and manual, JHEP 05 (2006) 026. arXiv:hep-ph/0603175.

[32] R. Brun, et al., GEANT Detector Description and Simulation Tool, CERN program library long writeup w5013 Edition (March 1994).

[33] X.-N. Wang, M. Gyulassy, HIJING: A Monte Carlo model for multiple jet production in p p, p A and A A collisions, Phys.Rev. D44 3501–3516.

[34] P. Z. Skands, Tuning Monte Carlo Generators: The Perugia Tunes, Phys.Rev. D82 074018.

[35] G. D'Agostini, A Multidimensional unfolding method based on Bayes' theorem, Nucl.Instrum.Meth. A362 487–498.

[36] V. Blobel, An Unfolding method for high-energy physics experiments (2002) 258–267arXiv:hep-ex/0208022.

[37] The method of reduced cross-entropy a general approach to unfold probability distributions, Nuclear Instruments and Methods in Physics Research Section A: Accelerators, Spectrometers, Detectors and Associated Equipment 340 (2) (1994) 400 – 412.

[38] V. Blobel, 8th CERN School of Computing - CSC '84, Aiguablava, Spain 9–22 Sep. (1984).

[39] G. D'Agostini, Bayesian inference in processing experimental data: Principles and basic applications, Rept.Prog.Phys. 66 1383–1420.

[40] A. Hocker, V. Kartvelishvili, SVD approach to data unfolding, Nucl.Instrum.Meth. A372 469–481.

[41] T. Adye, Unfolding algorithms and tests using RooUnfold arXiv:1105.1160.

[42] P. Amaudruz, et al., A Reevaluation of the nuclear structure function ratios for D, He, Li-6, C and Ca, Nucl.Phys. B441 3–11.

[43] K. Eskola, H. Paukkunen, C. Salgado, EPS09: A New Generation of NLO and LO Nuclear Parton Distribution Functions, JHEP 0904 065.

[44] J. Cronin, H. J. Frisch, M. Shochet, J. Boymond, R. Mermod, et al., Production of Hadrons with Large Transverse Momentum at 200-GeV, 300-GeV, and 400-GeV, Phys.Rev. D11 3105.

[45] I. Vitev, B.-W. Zhang, S. Wicks, The Theory and phenomenology of jets in nuclear collisions, Eur.Phys.J. C62 139–144.

[46] I. Vitev, S. Wicks, B.-W. Zhang, A Theory of jet shapes and cross sections: From hadrons to nuclei, JHEP 0811 093.

[47] C. A. Salgado, U. A. Wiedemann, Calculating quenching weights, Phys. Rev. D68 (2003) 014008.

[48] I. Vitev, Large angle hadron correlations from medium-induced gluon radiation, Phys.Lett. B630 (2005) 78–

84. arXiv:hep-ph/0501255, doi:10.1016/j.physletb.2005.09.082.

[49] N. Armesto, L. Cunqueiro, C. A. Salgado, Q-PYTHIA: A Medium-modified implementation of final state radiation, Eur.Phys.J. C63 679–690.

[50] L. Apolinario, N. Armesto, L. Cunqueiro, An analysis of the influence of background subtraction and quenching on jet observables in heavy-ion collisions, JHEP 1302 022.

[51] T. Renk, A Comparison study of medium-modified QCD shower evolution scenarios, Phys.Rev. C79 054906.

[52] T. Renk, YaJEM: a Monte Carlo code for in-medium shower evolution, Int.J.Mod.Phys. E20 1594–1599.

[53] J. Casalderrey-Solana, J. G. Milhano, U. A. Wiedemann, Jet Quenching via Jet Collimation, J.Phys. G38 035006.

[54] T. Renk, On the sensitivity of the dijet asymmetry to the physics of jet quenching, Phys.Rev. C85 064908.

[55] Y. Mehtar-Tani, C. A. Salgado, K. Tywoniuk, The Radiation pattern of a QCD antenna in a dense medium, JHEP 1210 197.

[56] Y. Mehtar-Tani, C. Salgado, K. Tywoniuk, Jets in QCD Media: From Color Coherence to Decoherence, Phys.Lett. B707 156–159.

[57] B. Abelev, et al., Centrality Dependence of Charged Particle Production at Large Transverse Momentum in Pb–Pb Collisions at $\sqrt{s_{\rm NN}} = 2.76$ TeV, Phys.Lett. B720 52–62.

[58] J. Casalderrey-Solana, J. G. Milhano, P. Q. Arias, Out of Medium Fragmentation from Long-Lived Jet Showers, Phys.Lett. B710 175–181.

[59] Y. Mehtar-Tani, J. Milhano, K. Tywoniuk, Jet physics in heavy-ion collisions, Int.J.Mod.Phys. A28 1340013.

[60] T. Renk, Biased Showers - a common conceptual Framework for the Interpretation of High pT Observables in Heavy-Ion Collisions arXiv:1212.0646.

[61] K. C. Zapp, F. Krauss, U. A. Wiedemann, A perturbative framework for jet quenching, JHEP 1303 080.